# LOS ALAMOS SCIENTIFIC LABORATORY
## OF THE UNIVERSITY OF CALIFORNIA ○ LOS ALAMOS    NEW MEXICO

NUMERICAL STUDY OF THE MOTIONS OF VARIOUSLY-SHAPED

SLABS ACCELERATED BY A HOT GAS

20000915 049

## LEGAL NOTICE

# LOS ALAMOS SCIENTIFIC LABORATORY
## OF THE UNIVERSITY OF CALIFORNIA    LOS ALAMOS    NEW MEXICO

**REPORT WRITTEN:** September 1958

**REPORT DISTRIBUTED:**  January 26, 1959

## NUMERICAL STUDY OF THE MOTIONS OF VARIOUSLY-SHAPED
## SLABS ACCELERATED BY A HOT GAS

by

Francis H. Harlow
Donald O. Dickman

# ABSTRACT

Numerical computations have been performed to determine the motion of a two-dimensional slab of initially-cold gas accelerated by a hot gas. The cold-gas slab had a sequence of holes, flanges, or other perturbations to its otherwise straight, parallel, infinite bounding walls. Information is also presented regarding pertinent characteristics of the computing method.

## I. Introduction

The Particle-in-Cell Method* for numerical study of two-dimensional hydrodynamics has been applied to a group of problems of the following nature:

Initially, an infinite, two-dimensional slab of cold gas separates vacuum on the right side from hot gas on the left, all at rest. One or the other of the contact surfaces is not straight; the cold gas has a periodic set of flanges, holes, or other disturbances. The problems are those of determining the subsequent development from the various initial configurations, with various density ratios between the gases.

In deriving the solutions presented here, both gases were considered to be nonviscous, polytropic and monatomic (specific heat ratio $\gamma = 5/3$). The cold gas was nonconducting of heat, while the hot one was isothermal in space and time.

The calculations were performed in rectangular coordinates with all characteristics being independent of z coordinate. The cold gas was aligned in the y direction. In the actual calculations, only a finite region of the system was studied, this being enclosed in a reflective two-dimensional box. Each calculation was concluded when the left and right boundaries began to perturb the results strongly. The top and bottom reflective walls ensured periodicity in the y direction, with the basic section in the calculation being one half of a period. Quantities such as energy, momentum, and mass are measured per unit thickness in the z direction.

The method of calculation is described briefly as follows: The rectangular region of study was divided into 1200 fixed, square cells, usually with 50 in the x direction and with 24 in the y direction. The gases were represented by mass points, initially 4 per cell, which moved according to a cell-wise finite-difference approximation to the differential equations of motion. The time-wise changes of the configuration proceeded by finite steps. In this form of the equations, mass, energy, and momentum conservation were still rigorously conserved, except for energy in the isothermal gas.

---

*F. H. Harlow, J. Assoc. Comp. Mach., 4, 137 (April, 1957); M. W. Evans and F. H. Harlow, Los Alamos Scientific Laboratory, Report LA-2139 (June, 1957).

Calculations were performed on the IBM Electronic Data Processing Machine, Type 704. An average of about 9 hours of computing time was required for each case.

In this report we present the results of the calculations together with discussions of some auxiliary calculations designed to show the limits of accuracy of the results and some properties of the calculation method. The results are, in a sense, preliminary; restrictions imposed by the computing machines, both in memory and in running time, prevented certain desirable explorations. Thus, it would have been useful to extend some of the calculations to an examination of the configurations at much later times. Besides requiring more computing time, such extensions would require greater machine memory for the larger regions to allow for expansion. Such larger regions can presently be obtained only at the expense of resolution. Another extension of interest would be in the direction of increasing the density of the cold gas in more of the calculations. This would greatly increase the running time also, because the time increment per cycle is fixed by stability requirements in the hot gas, while massiveness of the cold gas slows its motion.

One other direction of extension of the calculation would be towards more complicated equations of state (and the inclusion of viscosity) in the cold gas. We chose the simple materials for these studies for several reasons. First, the mixed-cell treatment in the computing method is more satisfactorily understood. Second, certain stages of the motion could be calculated by other methods and compared with the machine calculations. It is felt that the qualitative aspects of the motions of various other materials can be inferred from the results presented here.

Units were scaled in the calculations so that the height of the region studied was 24. In most cases there were 24 cells across this distance. The time scaling was determined by the specific internal energy of the hot (isothermal) gas, taken to be 0.9 units. Thus the sound speed was $c = \sqrt{(\gamma-1)(0.9)} = \sqrt{0.6} = 0.7746$, and the unit of time was the time required for a sound signal to go 0.7746 distance unit. The density of the hot gas always had the initial value of 4 mass units per unit area (per unit z-direction thickness). This corresponded to having 4 particles per cell, initially, each of unit mass. The density of the cold gas was variable; the ratio of its initial density to that of the hot gas is symbolized R.


## II.  Results of the Calculations

### A.  Succession of Rectangular Flanges on the Hot-Gas Side

In Fig. 1 is shown the initial and subsequent positions of the initially-cold

gas. The hot gas is on the left and the vacuum is on the right. The density ratio has R = 1. By t = 30 (just before collision with the right-hand wall of the system) the slab shows no sign of rupture. The flanges, however, are going to be pinched off, as there is a fairly large velocity gradient, with the bulk of material in the flanges moving to the right with about half the speed of the wall of gas.

The same initial configuration was studied for various other density ratios: R = 0.4, 2.5, and 10. In Fig. 2 are shown the configurations of the slab at times chosen to show that they all pass through a very similar shape, but at very different times. The problem with R = 2.5 was continued to much later times; the resulting configuration at t = 52, just before collision with the right hand wall, is shown in Fig. 3. At the narrowest neck in the slab, the density is about 3.5 times the original density, but the velocity gradient there is such as to indicate eventual breakage.

The initial flange was then elongated, as shown for the initial time in Fig. 4. Successive configurations show a greatly elongate flange, but little difference in the rest of the slab from that shown in Fig. 1.

The energies for the initial configuration of Fig. 1 are shown in Figs. 5, 6, and 7 as functions of time for the various density ratios. Drops in total internal energy result from expansion of the free surface after transit of the initial shock, and from expansion of the flange after initial compression. Behavior of the vertical kinetic energies is a strong indicator of the flange history. The first drop in this kinetic energy occurs when the shock hits the reflective surface (i.e., when the two shocks collide in the middle of the flange). This happens earlier than the time at which the total kinetic energy begins to drop, because the half width of the flange is less than the thinnest part of the slab thickness. The subsequent rise in vertical kinetic energy occurs when the return shock reaches the new outer-surface position of the flange wall.

Figure 8 shows the total internal and kinetic energies for the density ratio R = 1 in the configurations of Fig. 4. The vertical kinetic energy history is similar to those shown in Fig. 7, except that the initial rise is relatively much higher and the subsequent drop much more acute. The effect is shown in Fig. 8 where the first drop in kinetic energy is due to the loss of vertical kinetic energy in the flange. The late-time spurs on the energy curves arise because the slab has collided with the rigid wall on the right-hand side of the system.

Another set of calculations was performed in which the rectangular flanges were much wider than the intervening holes. Initial and subsequent configurations are shown in Fig. 9 for the density ratio R = 1. This calculation was also done with coarser zoning in the finite-difference mesh of cells in order that a much greater expansion could be calculated before the

slab collided with the right-hand wall. The results are shown, on the same space and time scale, in Fig. 10. The results at t = 20 agree with those shown in Fig. 9, except that some resolution of detail has been lost by the mesh coarseness. The final configuration at late times shows, at least qualitatively, that the slab could be expected to rupture. The energies for the two calculations are shown in Figs. 11, 12, and 13. The comparison in each case gives some indication of the accuracy of the results. Better comparisons with exact solutions are shown later in this report. The abrupt changes in total internal and kinetic energies at t = 32 are caused by collision of the slab with the right hand boundary of the calculation region.

## B.  Succession of Flanges on the Vacuum Side

The density ratio was R = 1. Initial and successive configurations are shown in Fig. 14. Effects of the flanges are not felt until relatively late times, and so there is only a small lateral propagation of signal along the slabs from the flanges; very little vertical kinetic energy is created. By the last time shown (t = 46) the mean rightward speed of the slab in the flange region is about 60% of the mean speed of the rest of the slab, and eventual rupture is suggested. Energies of the system are shown in Fig. 15. The problem can be solved exactly up to the time when the shock first breaks through to the other side of the slab. The exact result for both internal and kinetic energies is the same, also shown in Fig. 15. Further discussion of the exact solution is given later in this report.

## C.  Succession of Holes Through the Slab

Again the density ratio was R = 1. The initial and successive configurations are shown in Fig. 16. It is observed that the minimum width of the holes increases very little. The free surface of the escaping hot gas is also shown. (The finite size of the mass points does not allow the actual true surface to be seen; rather, one sees the representation of a moving isopycnic of appreciable density.)

## D.  Succession of Vacuum Pockets in the Hot Gas

The cold gas slab initially had perfectly plane, parallel boundaries. The hot gas next to it, however, had a succession of rectangular pockets of vacuum. Density ratio was R = 1. The results are shown in Fig. 17. Collapse of the hot gas into the vacuum pockets produced a jet into the gas slab, resulting in a strong contortion thereof. Early rupture is not indicated,

however, as there is very little hot gas in the pocket formed in the slab, and the slab material is beginning to move inward on the left side of the pocket. A small bubble of hot gas might eventually be able to break clear through.

## III. Discussion of the Results

### A. The Configurations

Data from which the configurations were drawn were obtained by a purely cell-wise examination of the presence or absence of material. The configurations could also be obtained more directly from a plot of the co-ordinates of the particles. The results would be the same to within the accuracy of the calculation. Nevertheless it is useful to examine the particle prints for several reasons. First, they show the compressions of the gas. Second, they show the nature of the irregularities of some of the boundaries. Both of these features are well shown in Fig. 18, which corresponds to the configuration at t = 38 shown in Fig. 17. Regions of high and low density can be distinguished at once. (The particles were originally spaced 4 per cell, one in the center of each quadrant.)

The configuration of mass points in Fig. 19 corresponds to that at t = 30 in Fig. 9. In this case, the nature of the surface instabilities is especially well exhibited.

### B. Accuracy of the Energy Curves

A comparison between the exact and calculated energy curves for the straight-line section of the interface has been shown in Fig. 15. The comparison is shown in more detail in Fig. 20. The datum points for energy are shown as they come from the calculation. The minor fluctuations can be traced to the discreteness of the mass points; such fluctuations have been removed from all the other energy curves of this report. It is observed that the energy errors can approximately be termed delays, with the internal energy being most affected.

These results are consistent with the results of fine and coarse zoning, as shown in Figs. 11 and 12. The finer zoning results (presumably more accurate) move the energy curves to the left (less delay), with the greater effect being noticed with the internal energy.

## C. Three Simplified Problems

Most of the initial configurations studied were constructed from three basic elements: straight line, concave right-angle corner, and convex right-angle corner (as viewed from the hot gas). Three machine calculations were performed to study in isolated form the interactions at the two types of corners; the interaction along the straight-line sections was discussed in the preceding section.

First, a concave corner was put into a square calculation region 34 cells wide, with the configuration having diagonal symmetry. Gases were the same as in all previous calculations; density ratio was $R = 1$. The initial and a later configuration are shown in Fig. 21 (a). At $t = 20$, a signal has just reached the right-hand and bottom boundaries. The approach to circular shape of the contact surface can be seen.

The same calculation was performed with a convex corner; results are shown in Fig. 21 (b). Next, the convex corner was rotated by 90°. Sides adjacent to the corner were represented by cell-wise steps -- see Fig. 21 (c). This again represents a right-hand corner because of the reflective boundary conditions along the edges of the region of calculation. The nature of the corner spike and adjacent sides was in very close agreement with the results shown in Fig. 21 (b). This serves greatly to increase confidence in the configuration results presented in this report; it may be that configurations are accurate in all cases, to within the width of a cell.

Energies calculated for these three problems are shown in Figs. 22, 23, and 24. The straight line, in each case, is the kinetic and internal energy curve that has been calculated exactly as though the boundary between the gases were one straight line with no corner, but of the same total length as the initial one with corner.


## D. Pertinent Additional Information About the Computing Method

Previous reports have mentioned the fact that difficulties may arise in the Particle-in-Cell Method whenever the mean material speed relative to the computation mesh is small compared with the sound speed. Since that situation occurs in the hot gas in the problems discussed in this report, it was necessary to examine the matter in somewhat more detail than had been attempted previously, For this purpose, two computations were performed.

In the first computation, the mesh was a square region with 15 cells on a side. The same hot isothermal gas used in all the calculations was put into the entire mesh with uniform distribution of 4 particles per cell, except that one corner cell was initially empty and one of its neighbors had

8 particles. No cold gas was put in. The gas was initially at rest. Thus there was created a region of "perturbed stagnation" which previously has been considered to be too unstable to allow. The computing was then carried out in usual fashion for enough elapsed time to allow a sound signal to propagate about 3 times across the mesh. By this time (t = 67.5) the system had nearly reached equilibrium. The resulting distribution of number of particles per cell is shown in Fig. 25. The distributions of horizontal and vertical velocity components are shown in Figs. 26 and 27. (The two cells originally perturbed were aligned vertically.) The speed of sound in the gas is 0.7746, so that it is very improbable that any cell would ever attain sound speed.

The total kinetic energy resulting from the calculation is shown as a function of time in Fig. 28. The individual datum points are shown together with an approximate mean. Scatter of the points is very much greater than scatter of the energy points of the initially-cold gas in the other calculations. By latest times (approximate equilibrium), the kinetic energy of this disordered motion has become about 3% of the total energy of the gas. Horizontal momentum of the system as a function of time is shown in Fig. 29.

Exactly the same computation was again performed, except that the gas was not restricted to be isothermal; instead, energy was perfectly conserved. The computation was run about half as far as the other one, during which time it was observed that the rise in kinetic energy was about half as fast, and the horizontal-momentum fluctuations had about half the amplitude, as in the isothermal calculation.

One feature of the computation, which was different from procedure previously followed, had some effect in stabilizing these calculations. Particles approaching the reflective boundary were allowed to reflect when they crossed (as they could because there was no reflective "velocity weighting" at the boundary). They then repartitioned as though entering from a reflective cell. This avoided "boundary catastrophes."* There was not, however, any "artificial viscosity" added beyond that which automatically arises as a consequence of the computing method.**

--------

*See LA-2139, page 17, for a further description.

**Ibid., page 16.
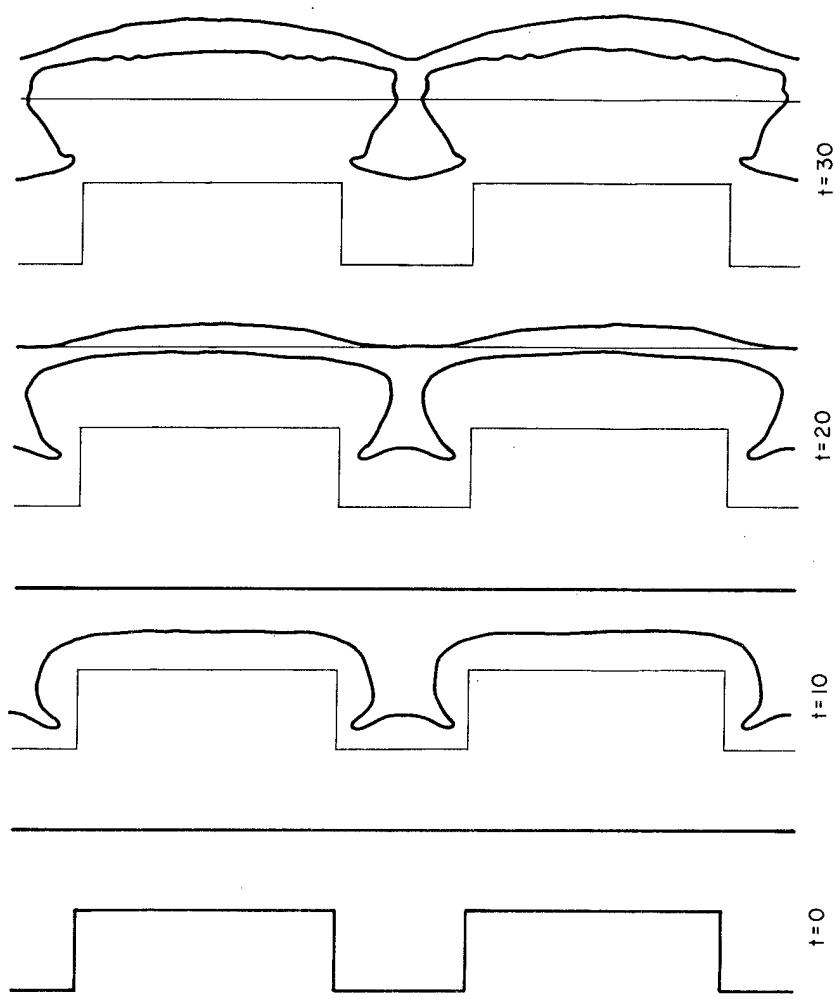
Fig. 1 Successive configurations of gas slab with internal flanges; density ratio R = 1.
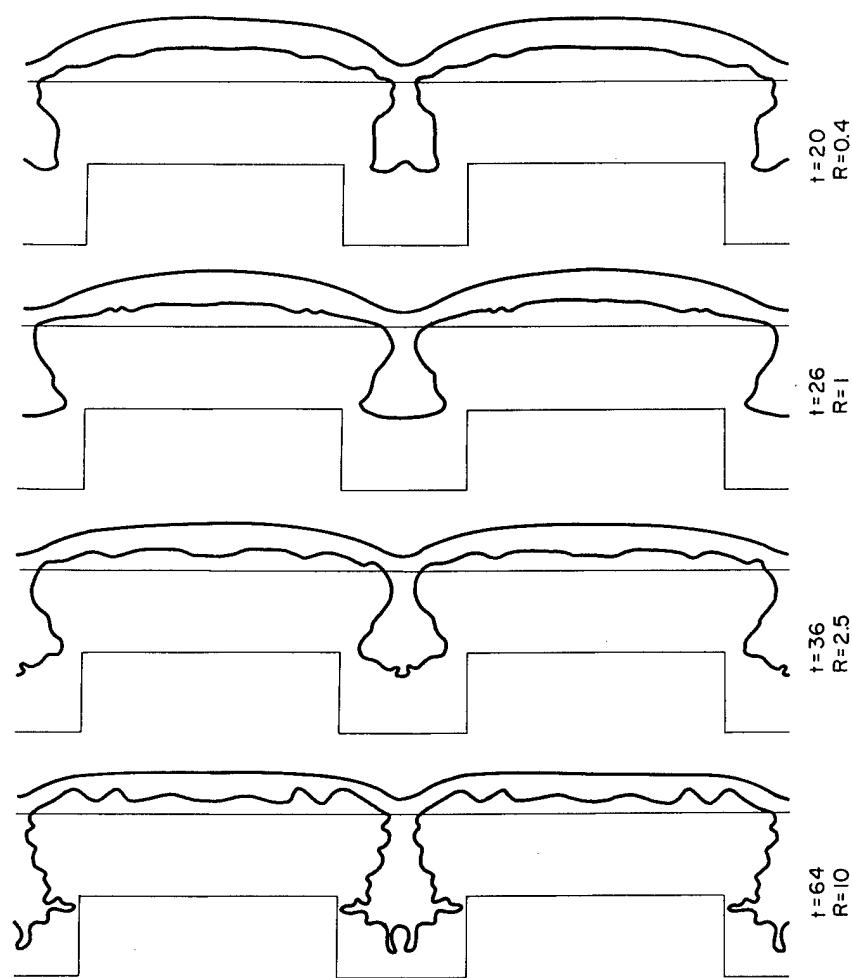
Fig. 2 Configurations arising from the same initial configurations as in Fig. 1, but for various density ratios.
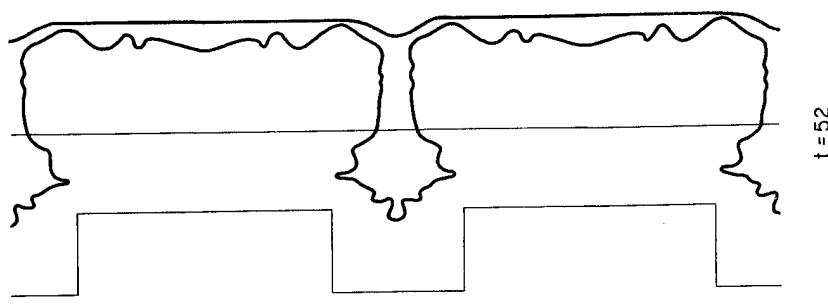
t = 52

Fig. 3 The configuration at time t = 52 of the slab with R = 2.5 shown in Fig. 2 at time t = 36.

Fig. 4 Successive configurations of gas slab with density ratio R = 1.

t=36

t=24

t=12

t=0
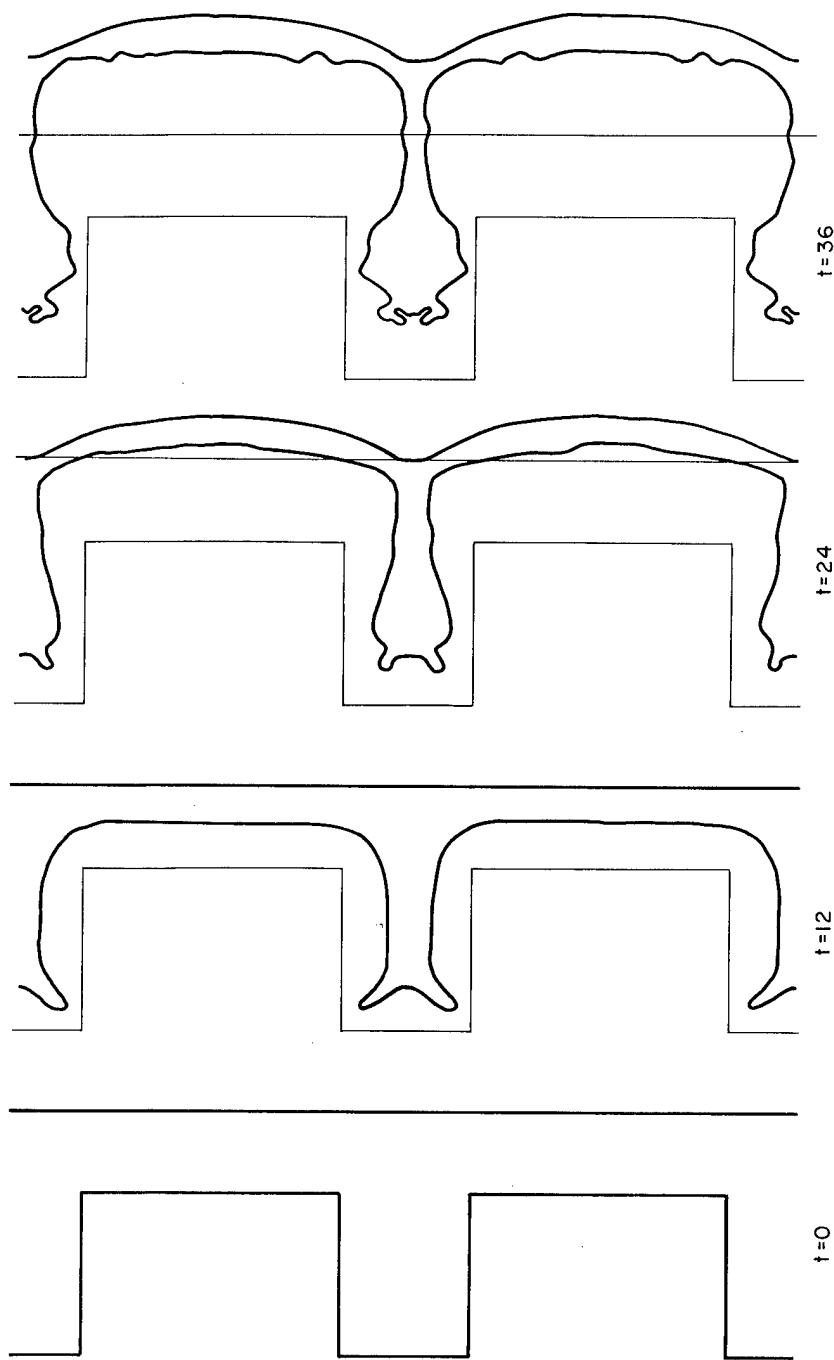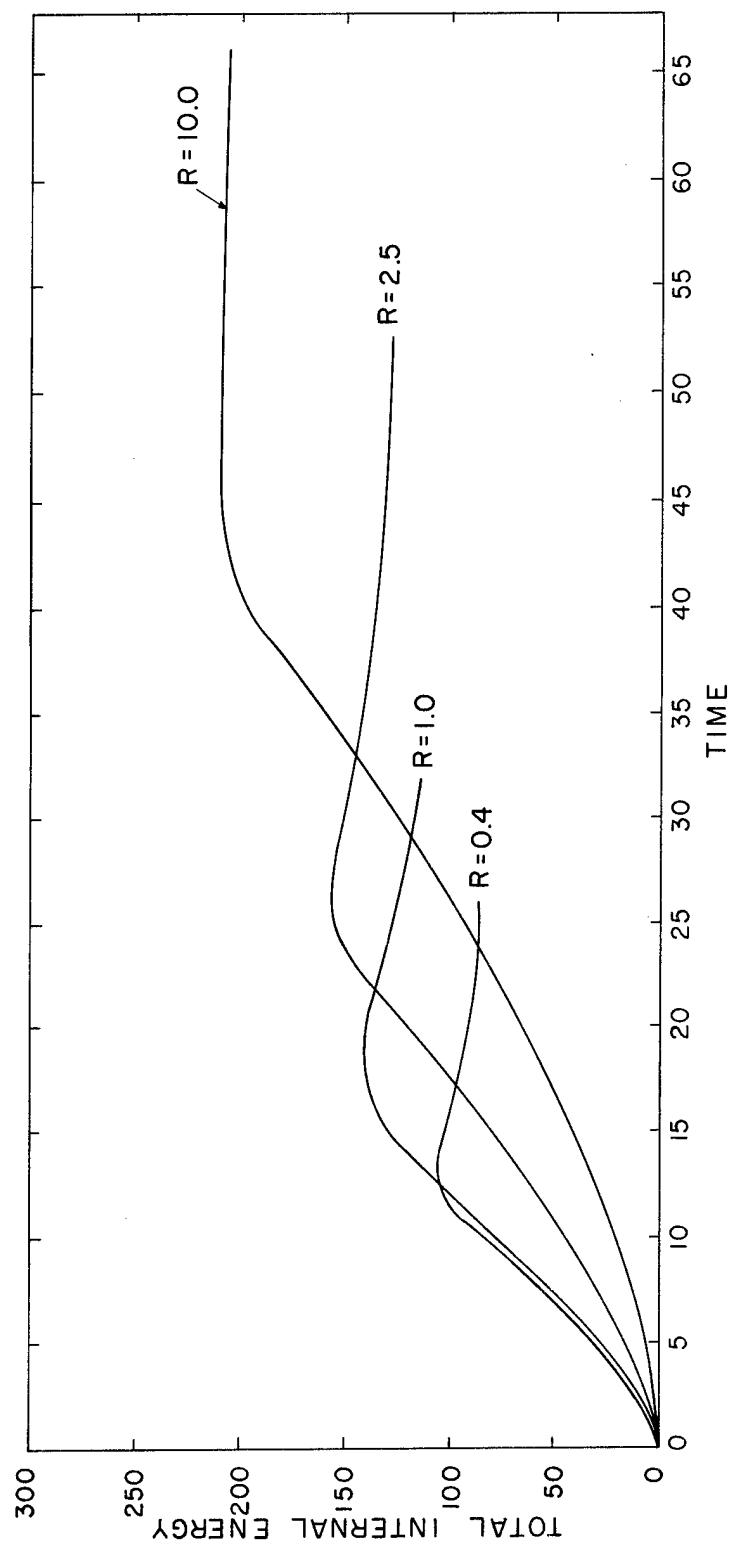
Fig. 5   Total internal energy of one basic section of the slab, shown as a function of time for various density ratios; initial configuration as in Fig. 1.
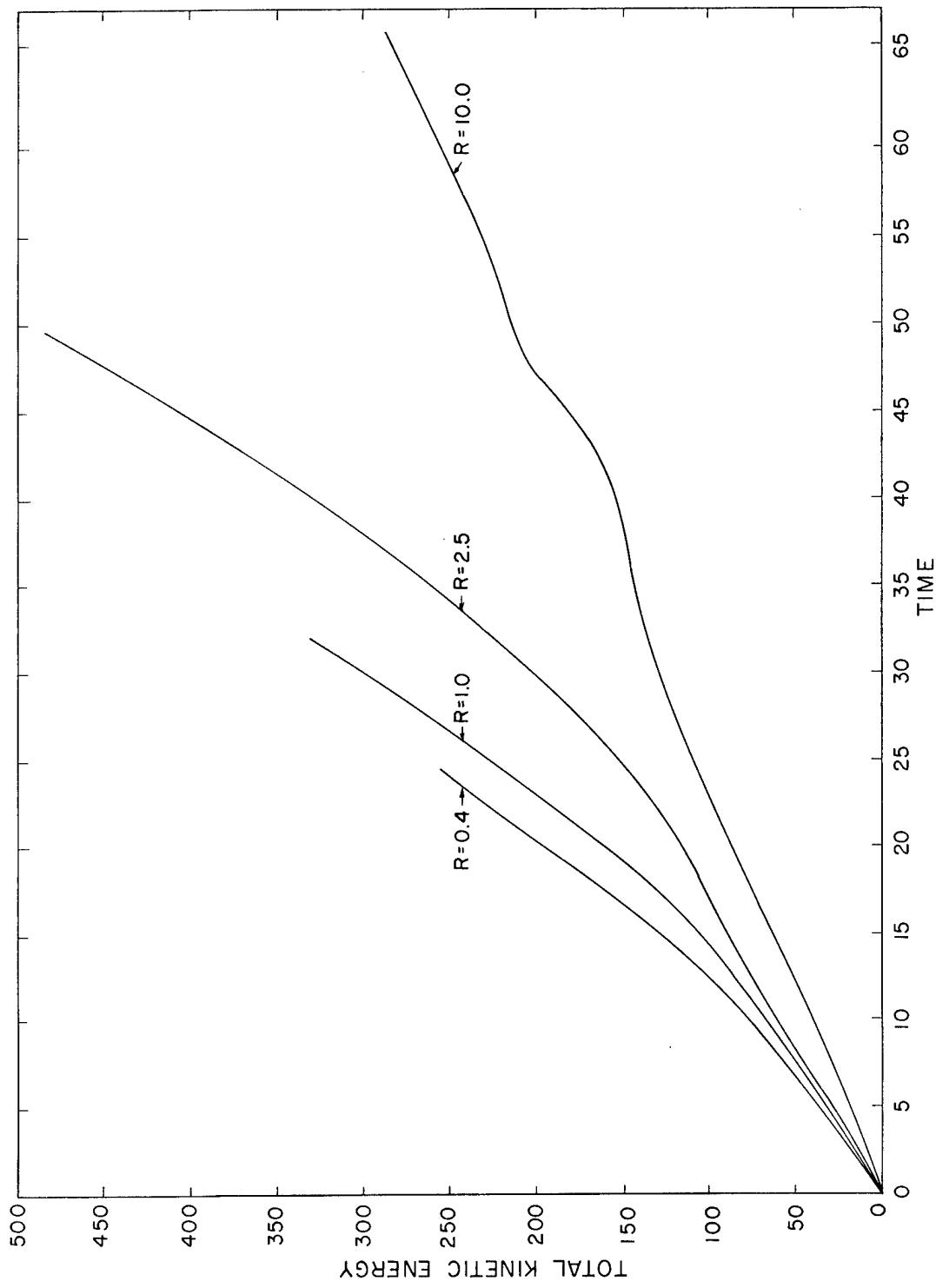
Fig. 6  Total kinetic energy of one basic section of the slab, shown as a function of time for various density ratios; initial configuration as in Fig. 1.
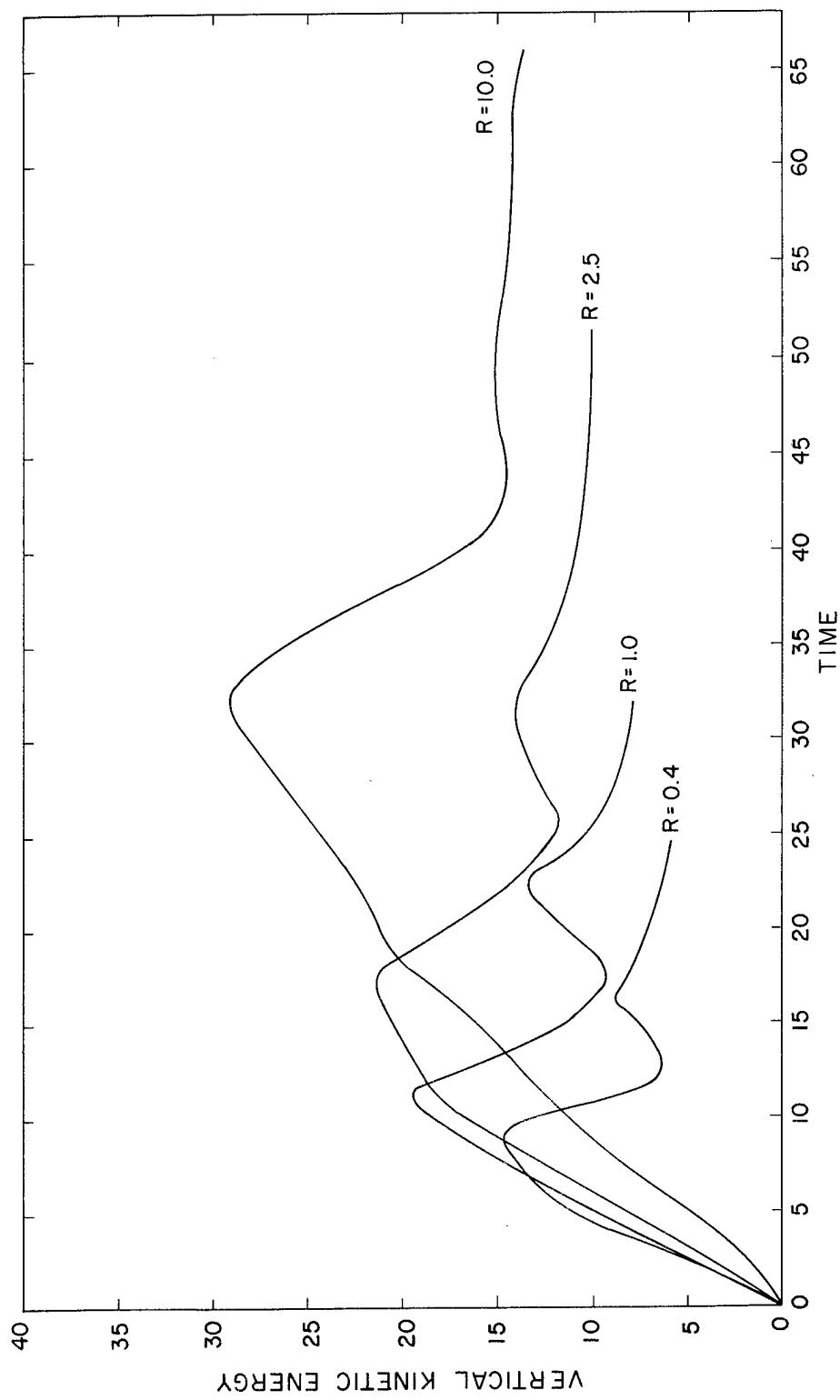
Fig. 7  Vertical kinetic energy of one basic section of the slab, shown as a function of time for various density ratios; initial configuration as in Fig. 1.
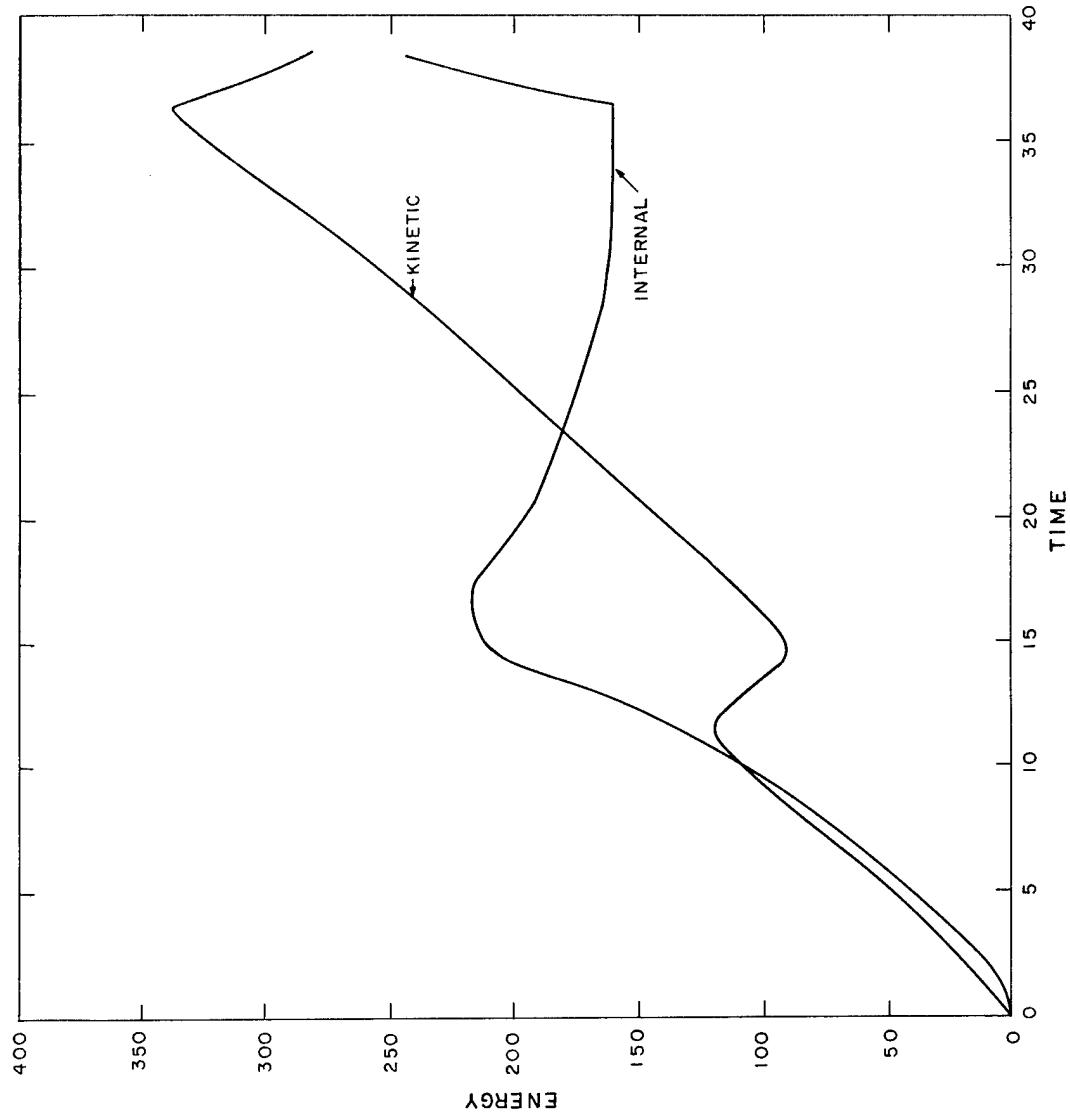
Fig. 8  Total internal and kinetic energies of one basic section of the slab, for the density ratio R = 1 in the configurations of Fig. 4.
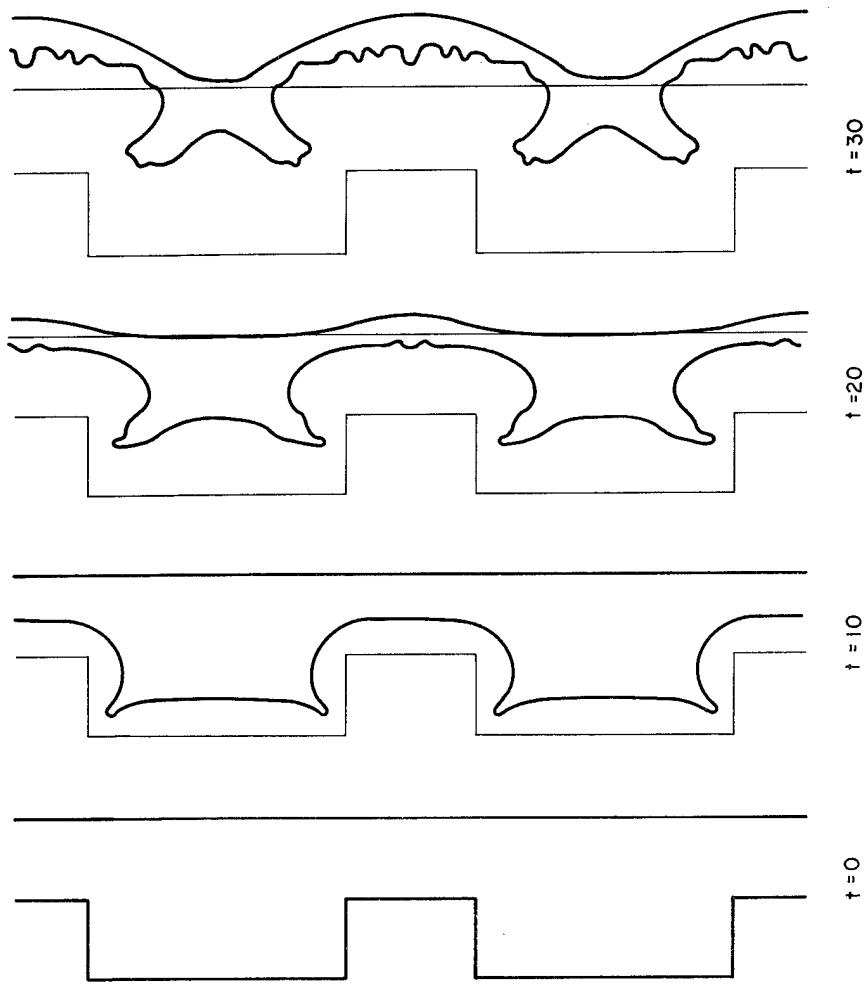
Fig. 9  Successive configurations of gas slab with wide internal flanges; density ratio R = 1.
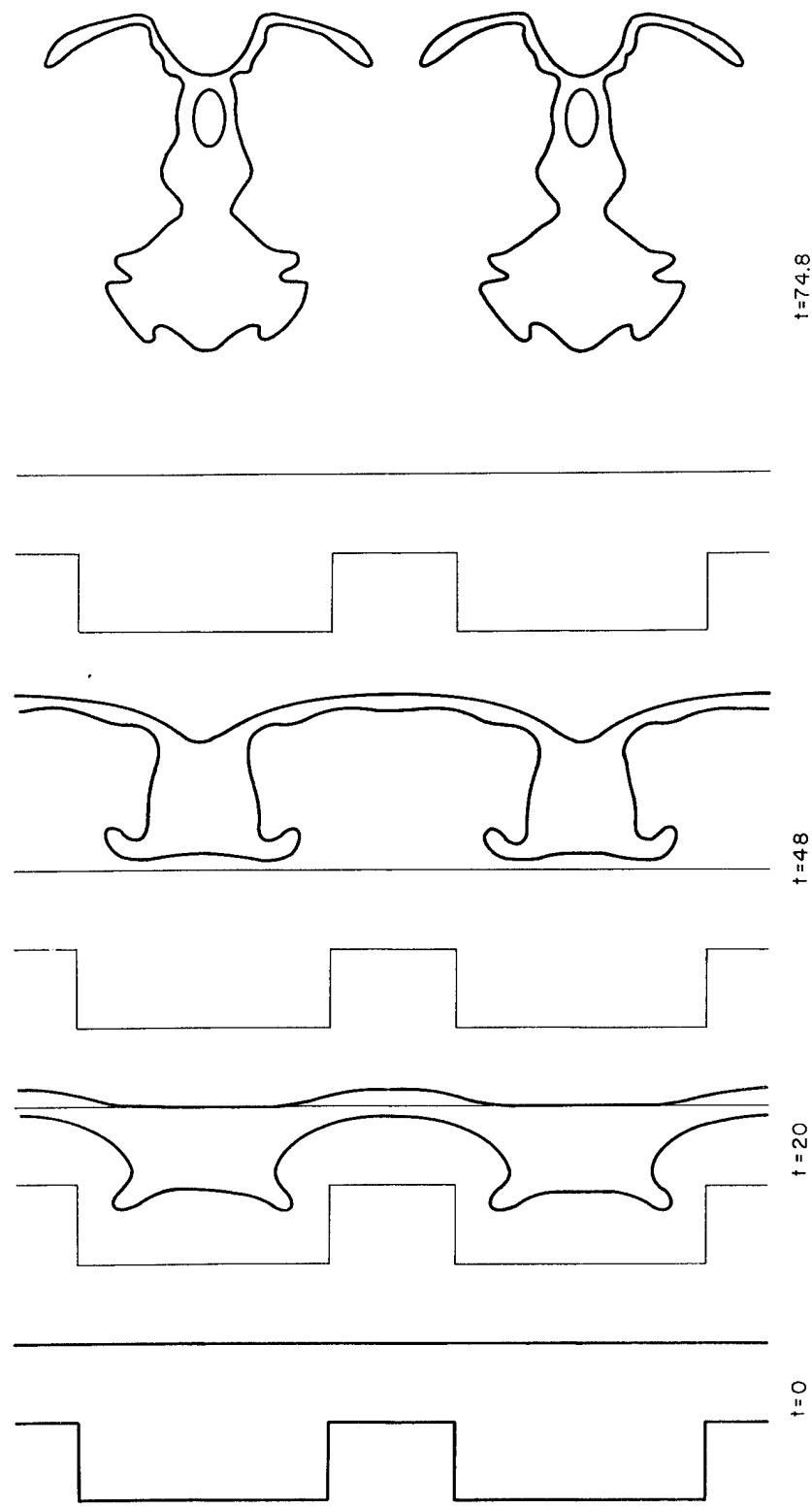
Fig. 10  Same calculation as that represented in Fig. 9, but with coarser zoning to allow greater motion of the slab.
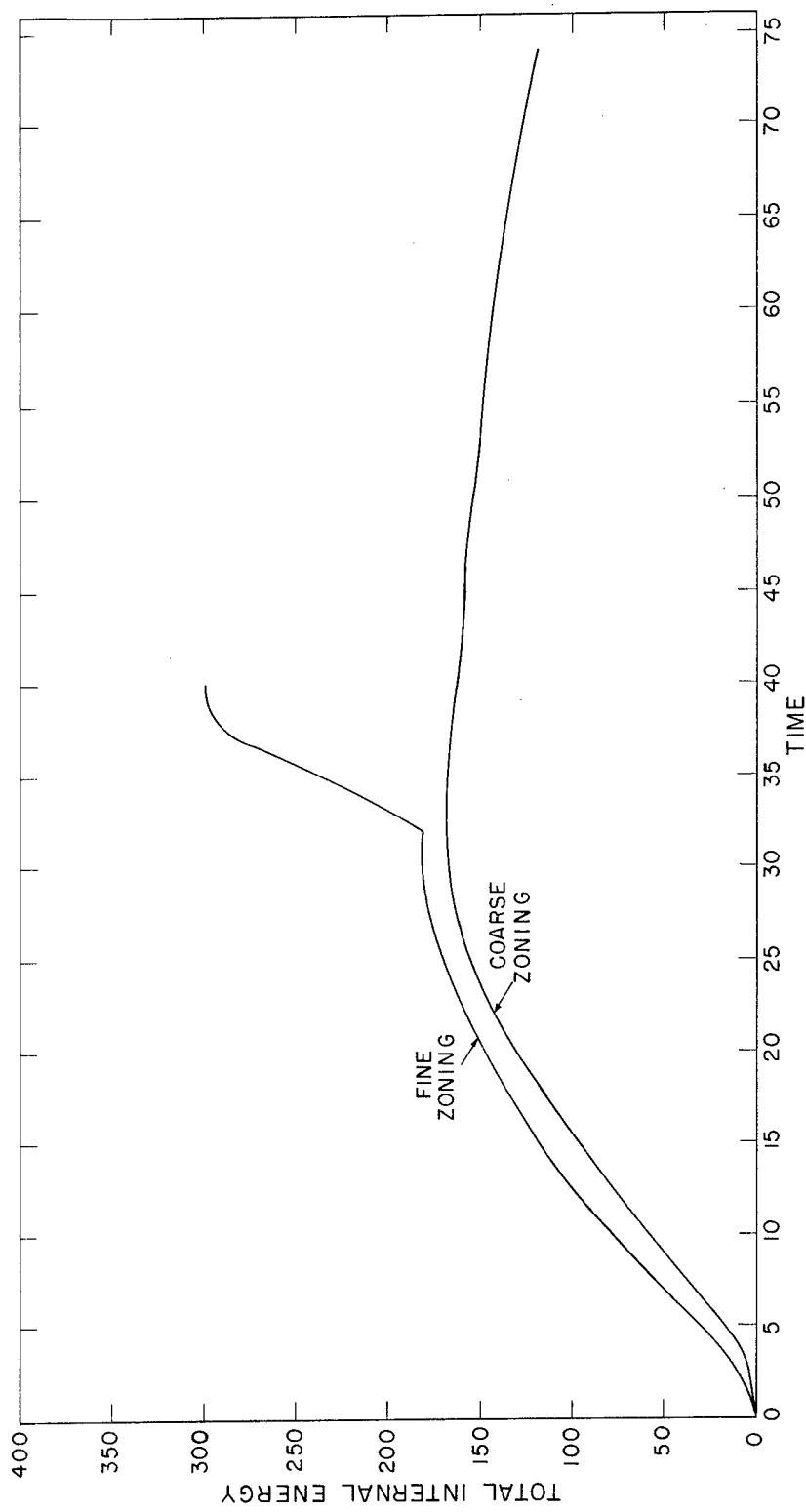
Fig. 11  Total internal energy of one basic section of the slab, shown as a function of time, for the calculations shown in Figs. 9 and 10.
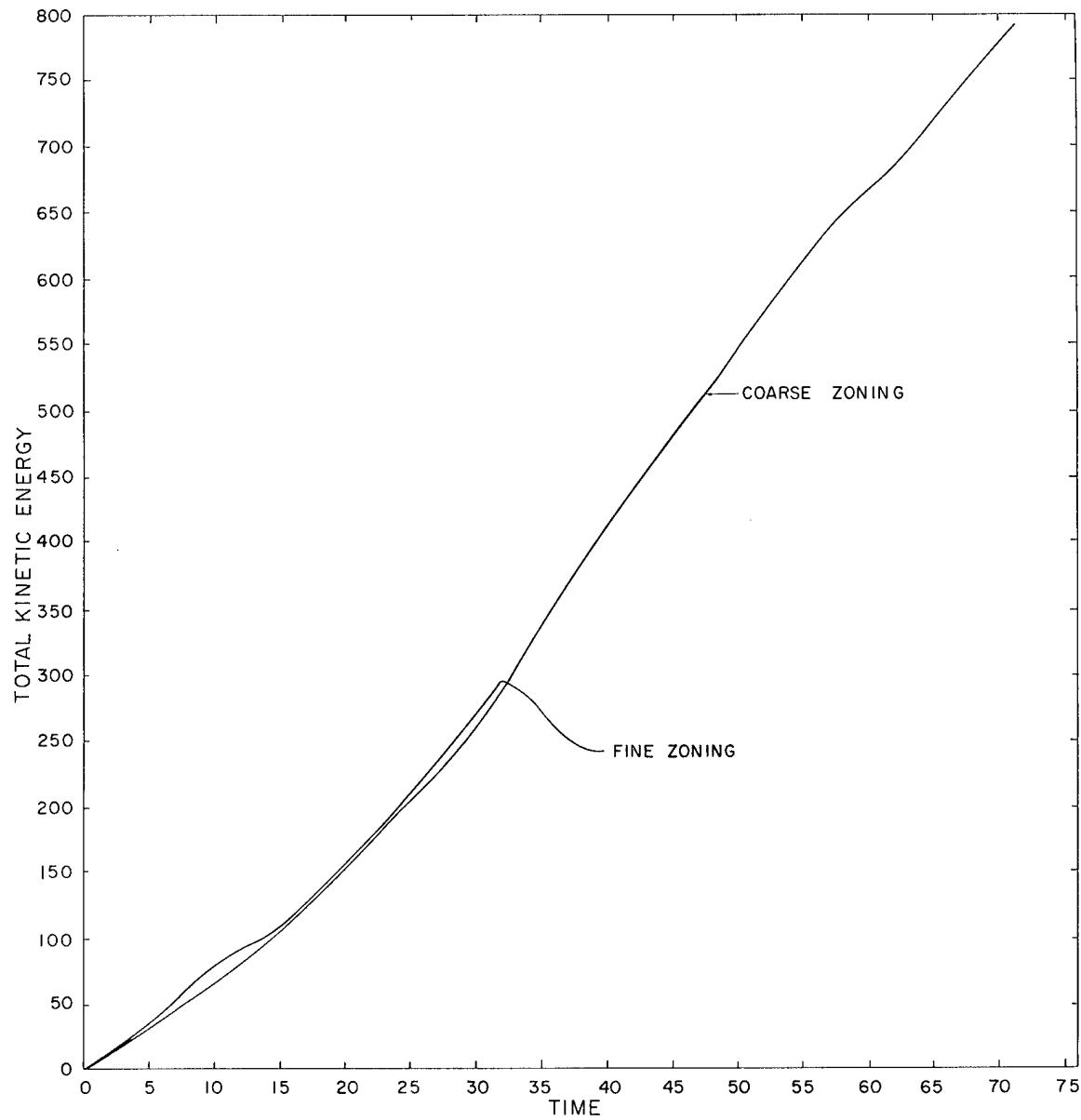
Fig. 12  Total kinetic energy of one basic section of the slab, shown as a
function of time, for the calculations shown in Figs. 9 and 10.
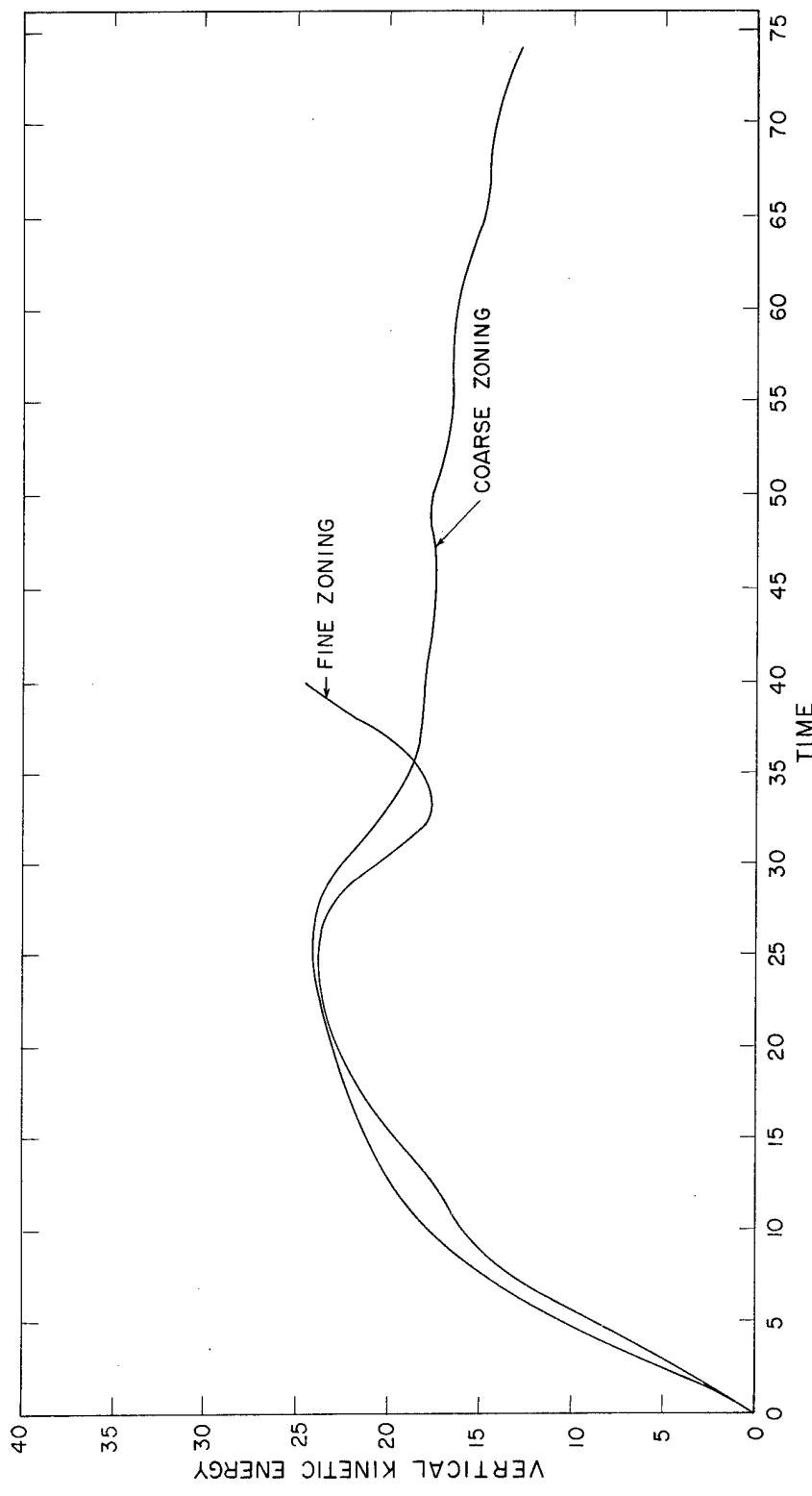
Fig. 13   Vertical kinetic energy of one basic section of the slab, shown as a function of time, for the calculations shown in Figs. 9 and 10.
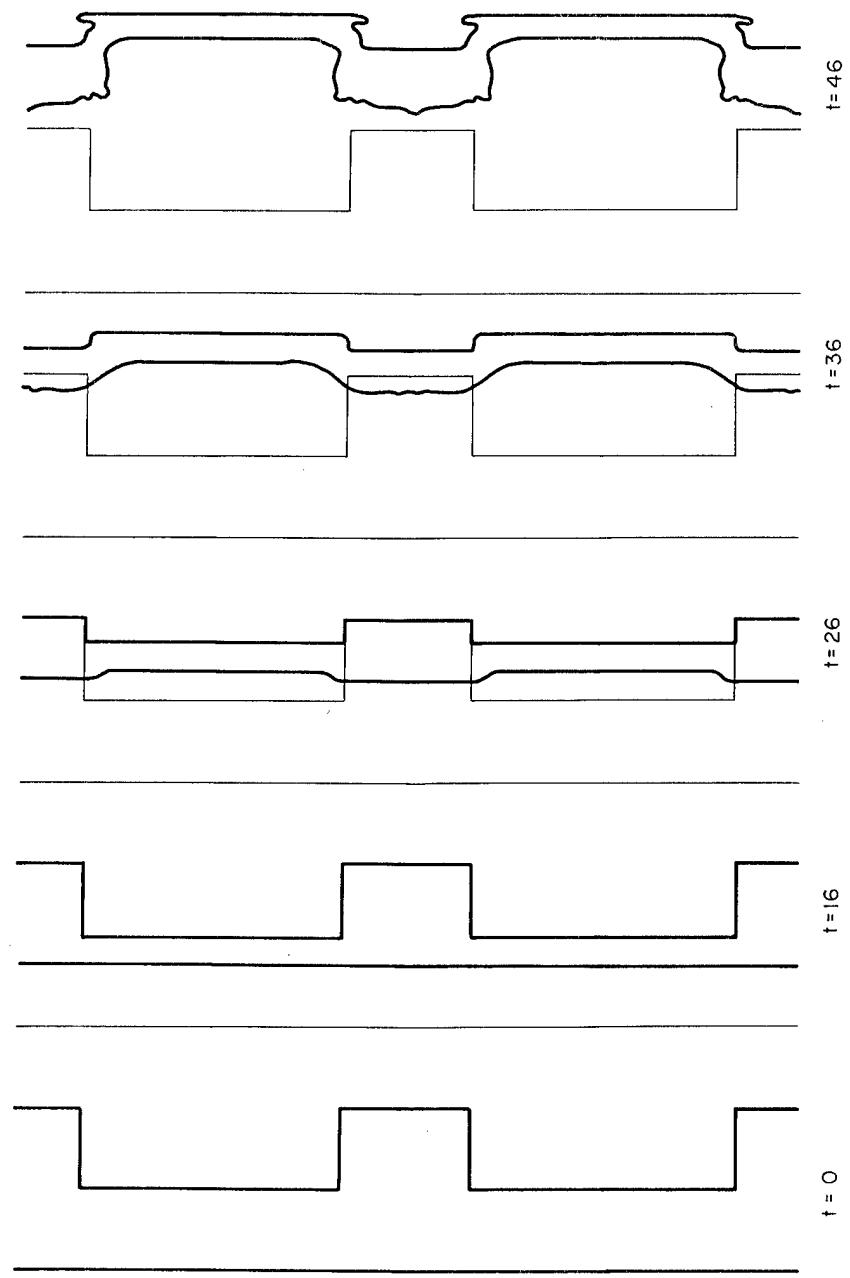
Fig. 14 Successive configurations of gas slab with external flanges; density ratio R = 1.
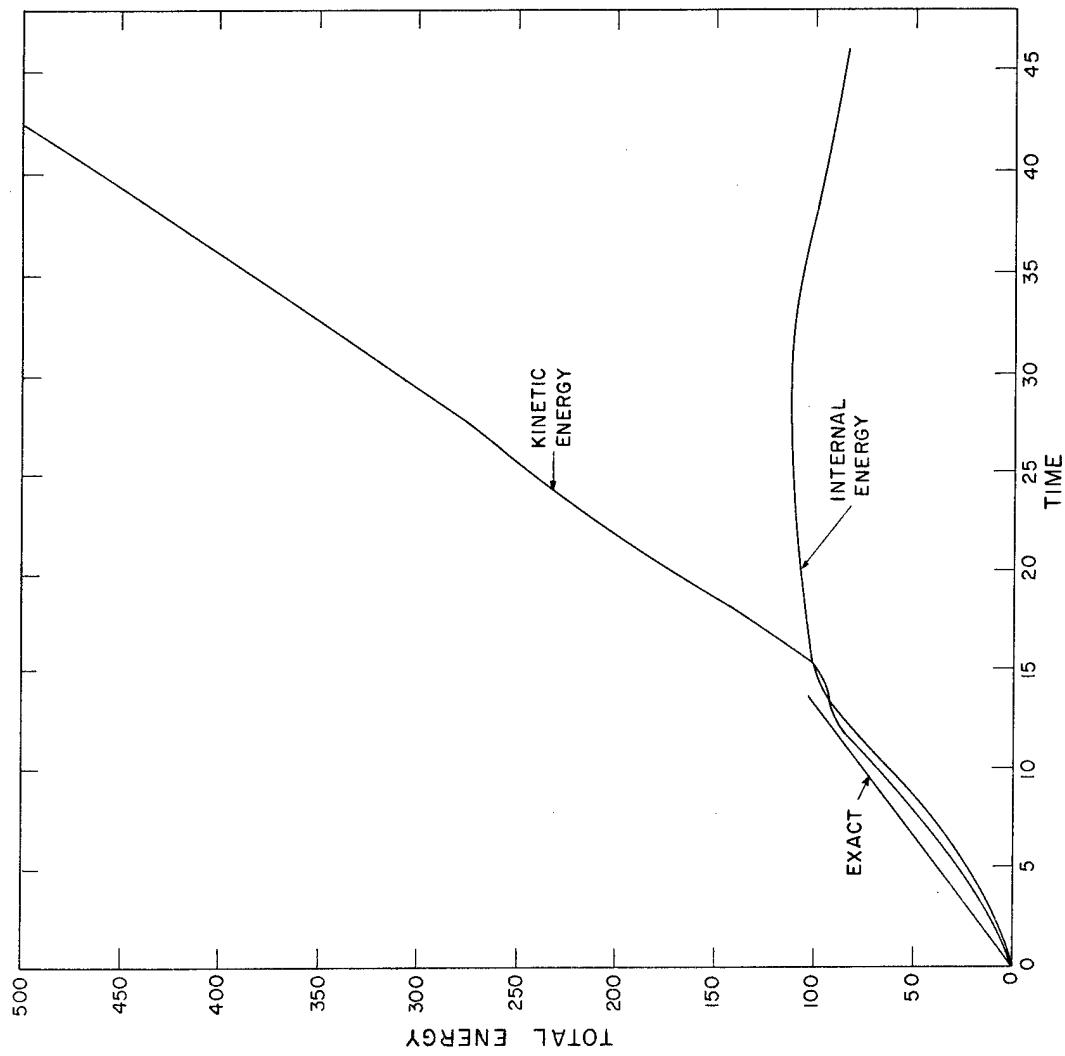
Fig. 15  Total internal and kinetic energies of one basic section of the slab, shown as a function of time, for the calculation shown in Fig. 14.  Exact solution refers to both energies.
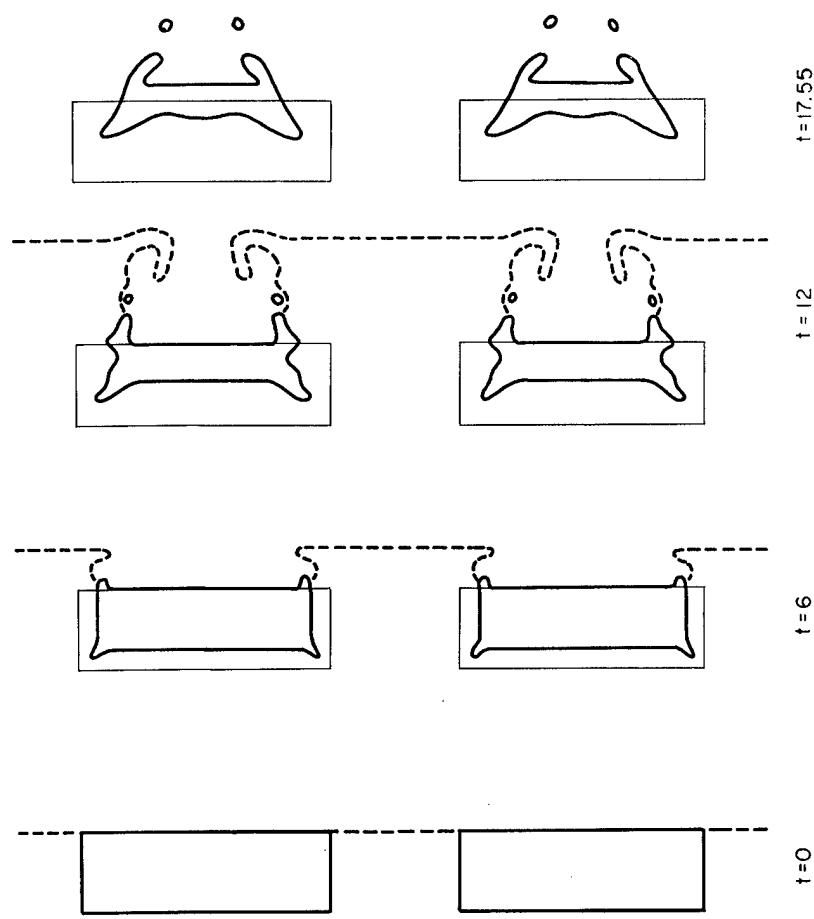
Fig. 16 Successive configurations of gas slab with holes; density ratio R = 1. Dashed line shows free-surface position of hot gas.

t=0   t=6   t=12   t=17.55
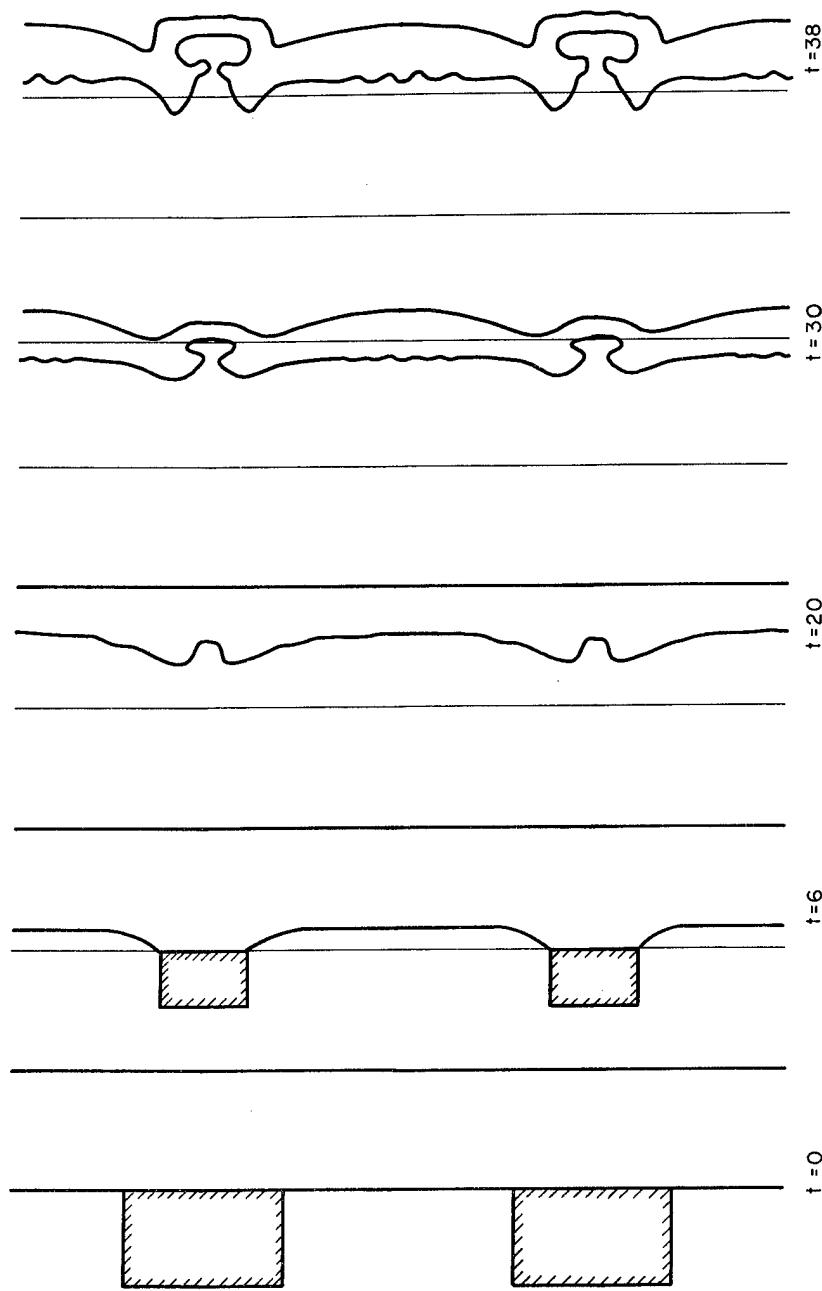
Fig. 17  Successive configurations of gas slab with density ratio R = 1.  Cross–hatched regions repre–
sent vacuum pockets in the hot gas.
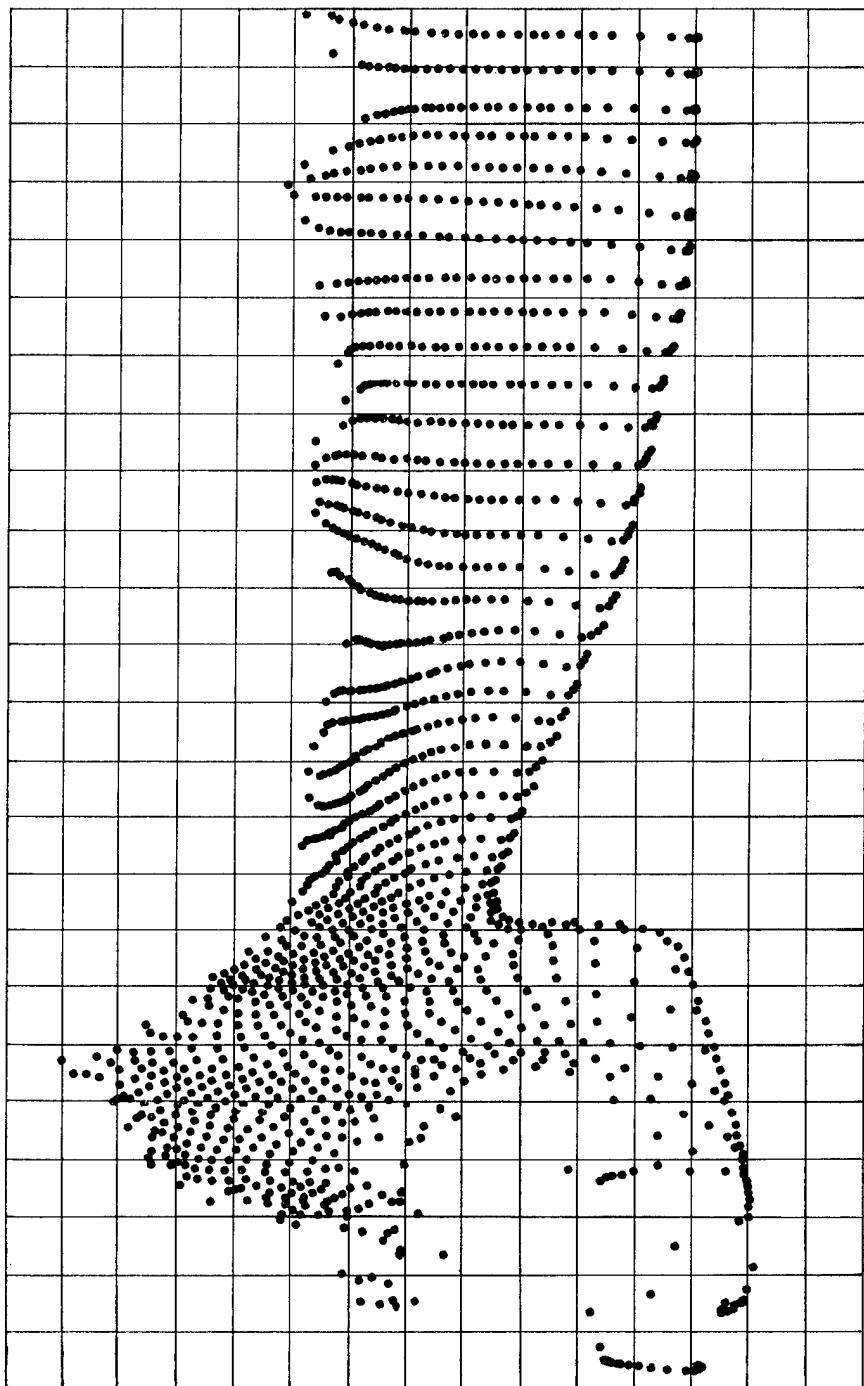
Fig. 18   Configuration of mass points in one basic section of the gas slab,
corresponding to the configuration at t = 38 in Fig. 17.  Grid lines
show the cell size.
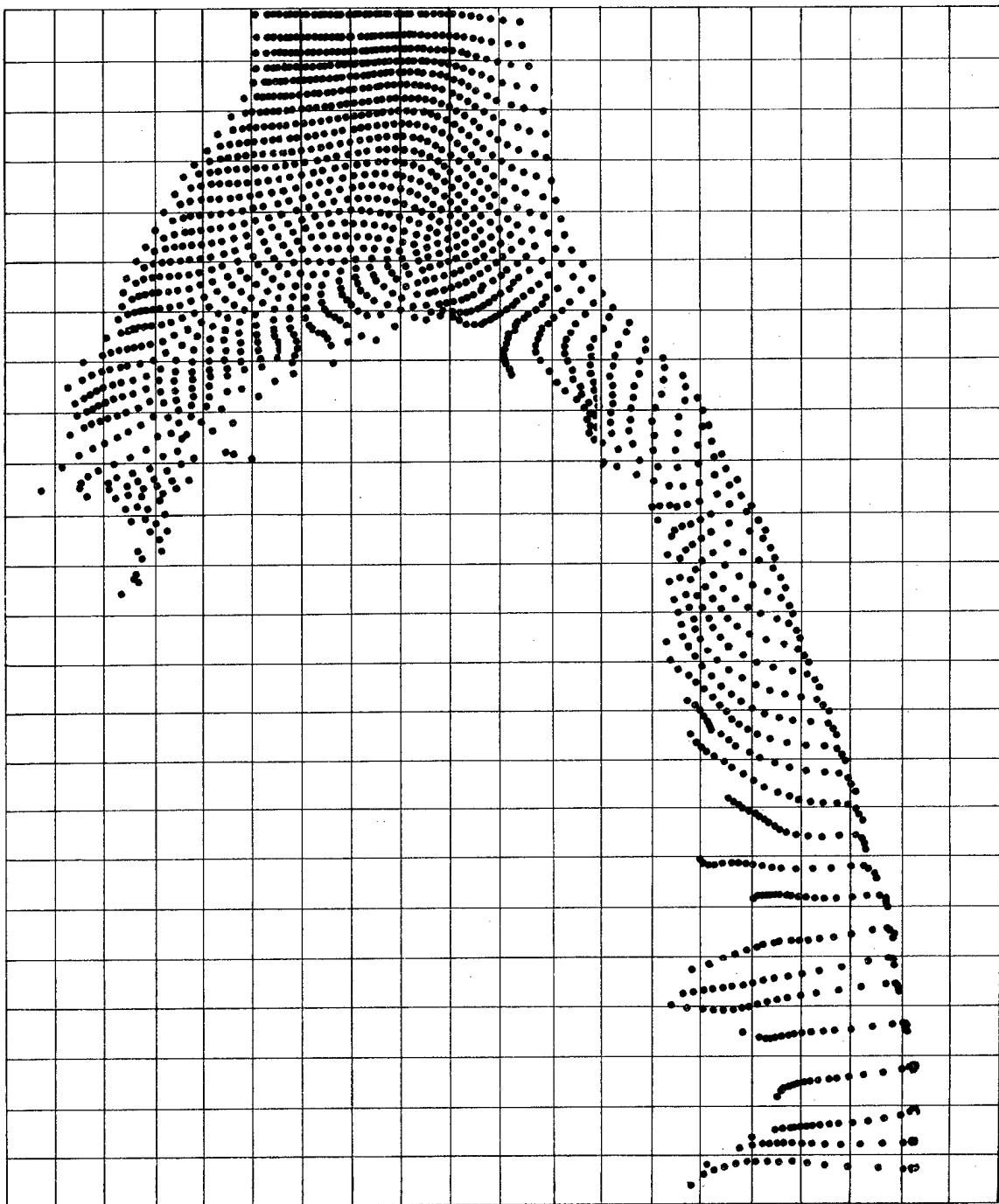
Fig. 19  Configuration of mass points in one basic section of the gas slab,
corresponding to the configuration at t = 30 in Fig. 9. Grid lines
show the cell size.
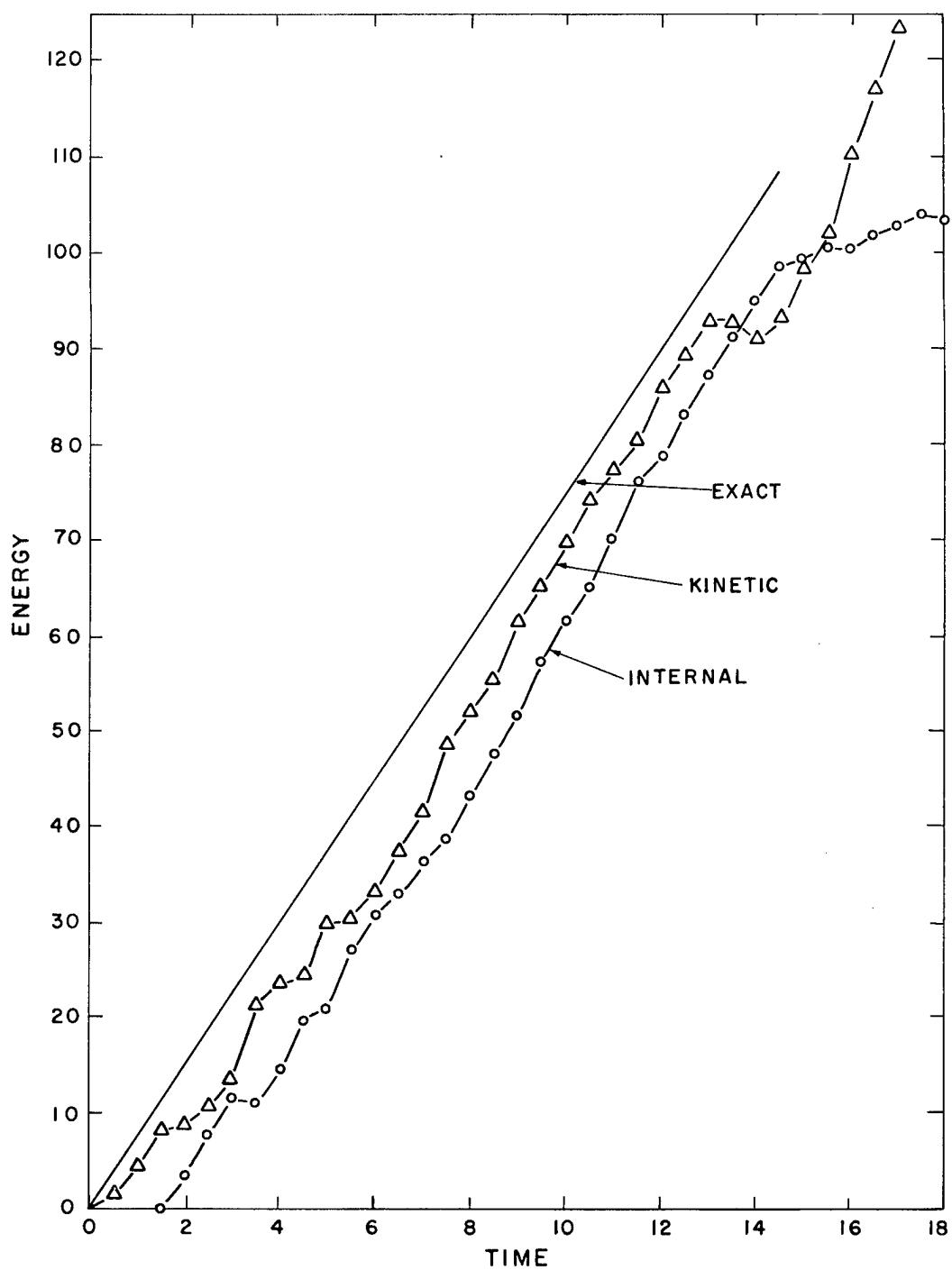
Fig. 20 Comparison of calculated and exact internal and kinetic energies --
a detailed examination of the early part of the curves in Fig. 15.
Individual points are data direct from the calculation.
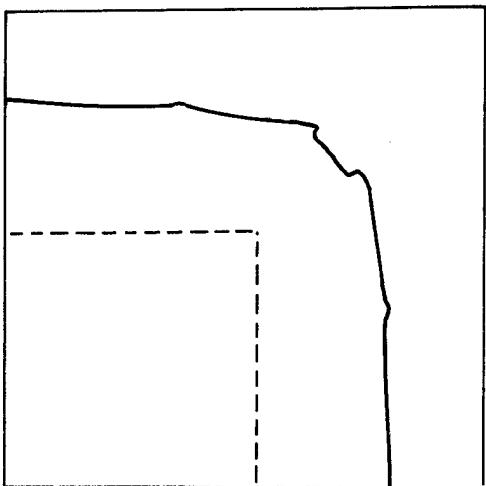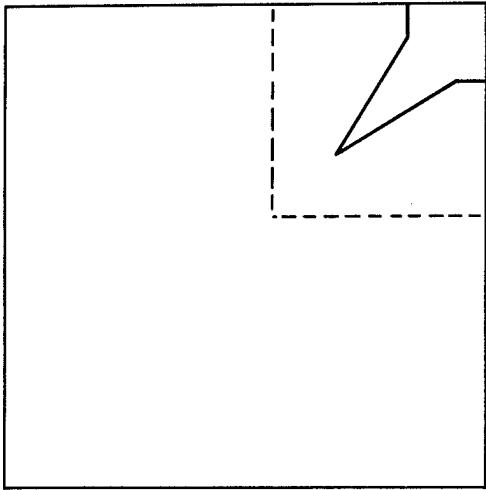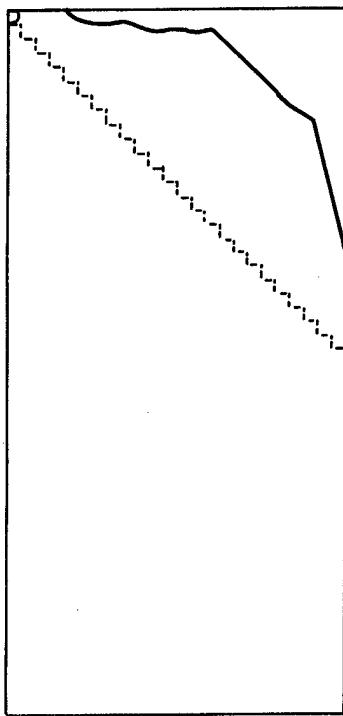
Fig. 21 Configurations in the interaction of the hot gas (towards the upper left) with the cold gas for density ratio R = 1: (a) concave corner, (b) convex corner, (c) convex corner rotated by 90°. Dotted lines show initial configurations; solid lines show configurations at t = 20.
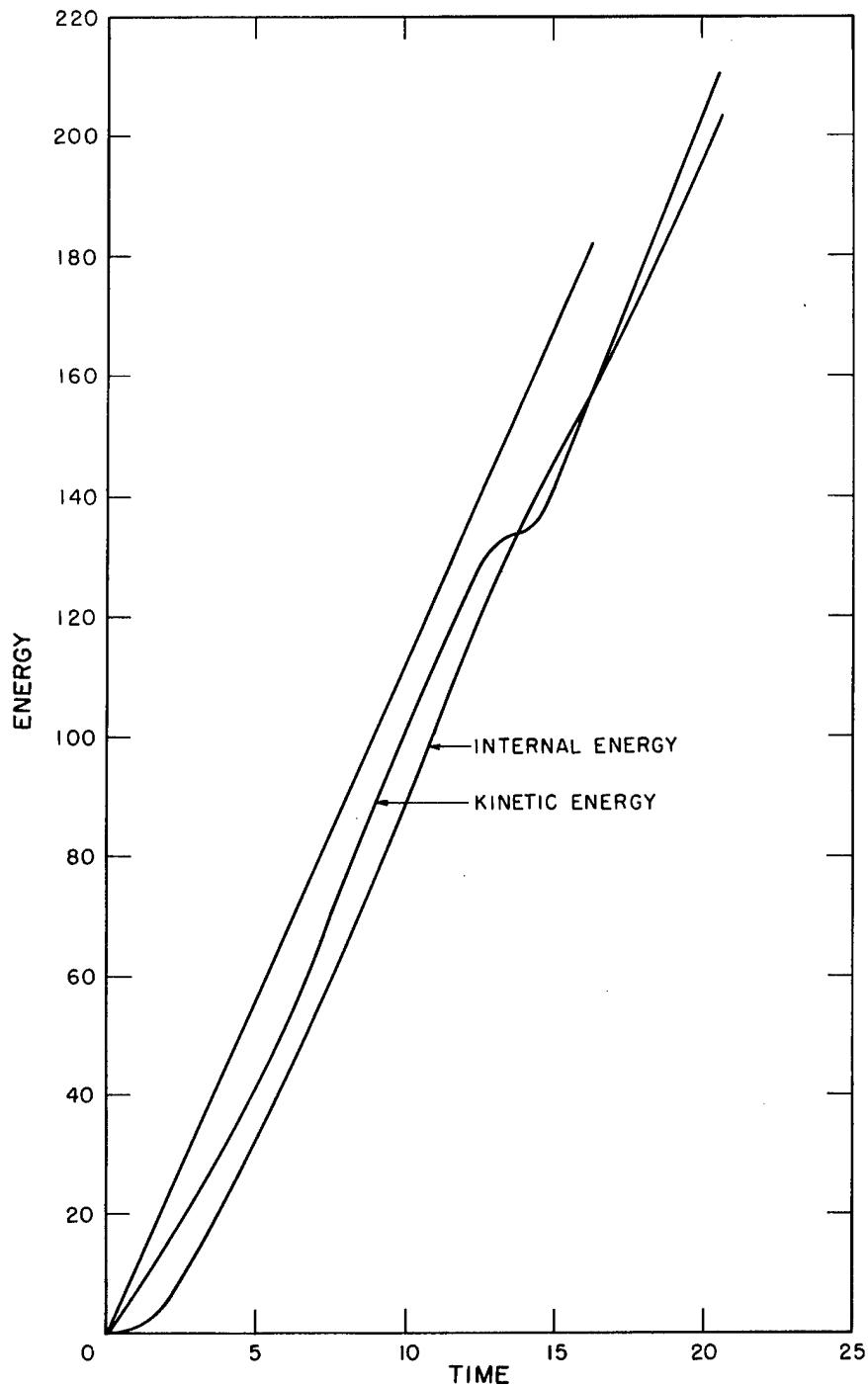
Fig. 22   Total internal and kinetic energies of the initially-cold gas for the calculation shown in Fig. 21 (a). Straight line for comparison is the simple-compression curve.
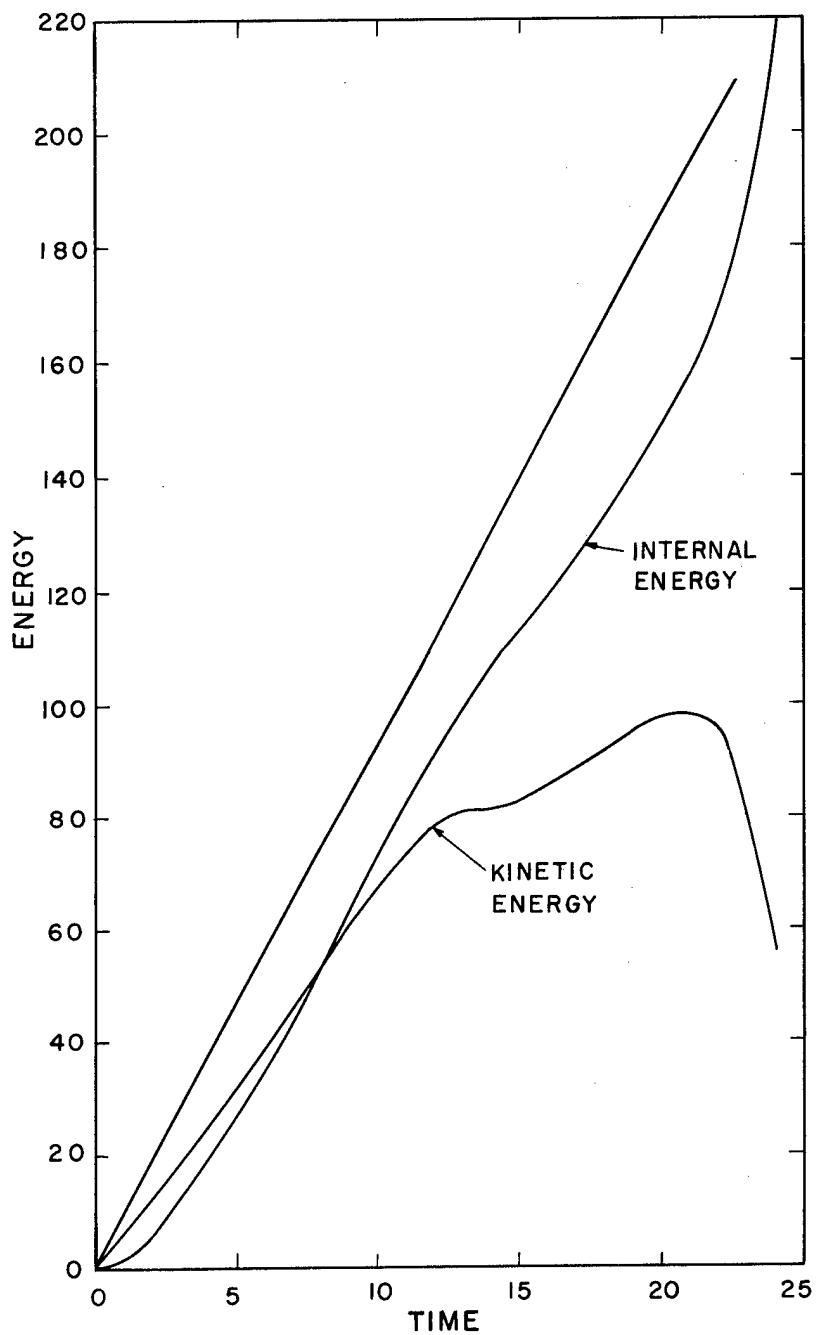
Fig. 23 Total internal and kinetic energies of the initially-cold gas for the calculation shown in Fig. 21 (b). Straight line for comparison is the simple-compression curve. Strong deflections of the curves at t = 21 arise from collision of the shocks with the rigid walls of the calculation region.
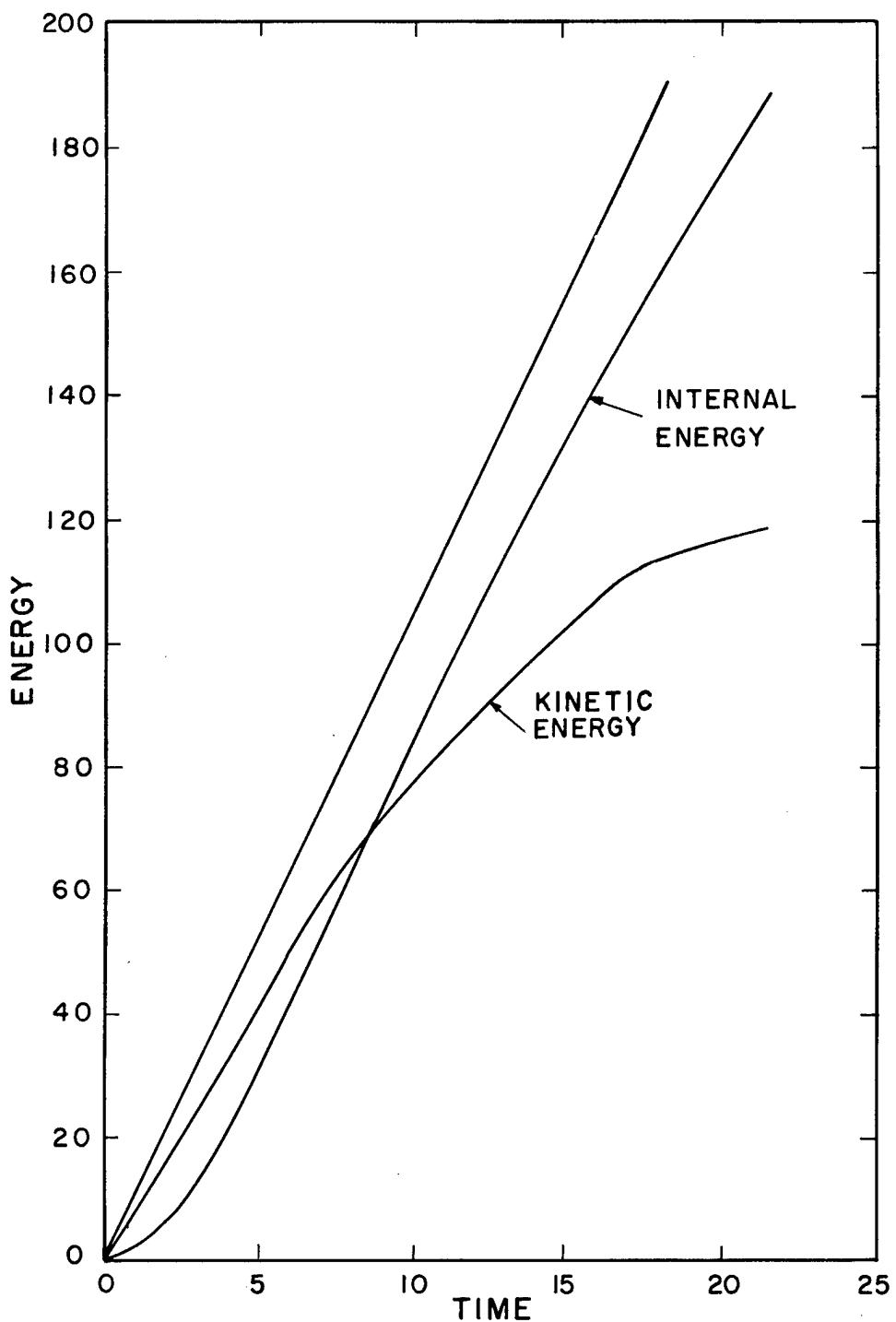
Fig. 24  Total internal and kinetic energies of the initially-cold gas for the calculation shown in Fig. 21 (c).  Straight line for comparison is the simple-compression curve.
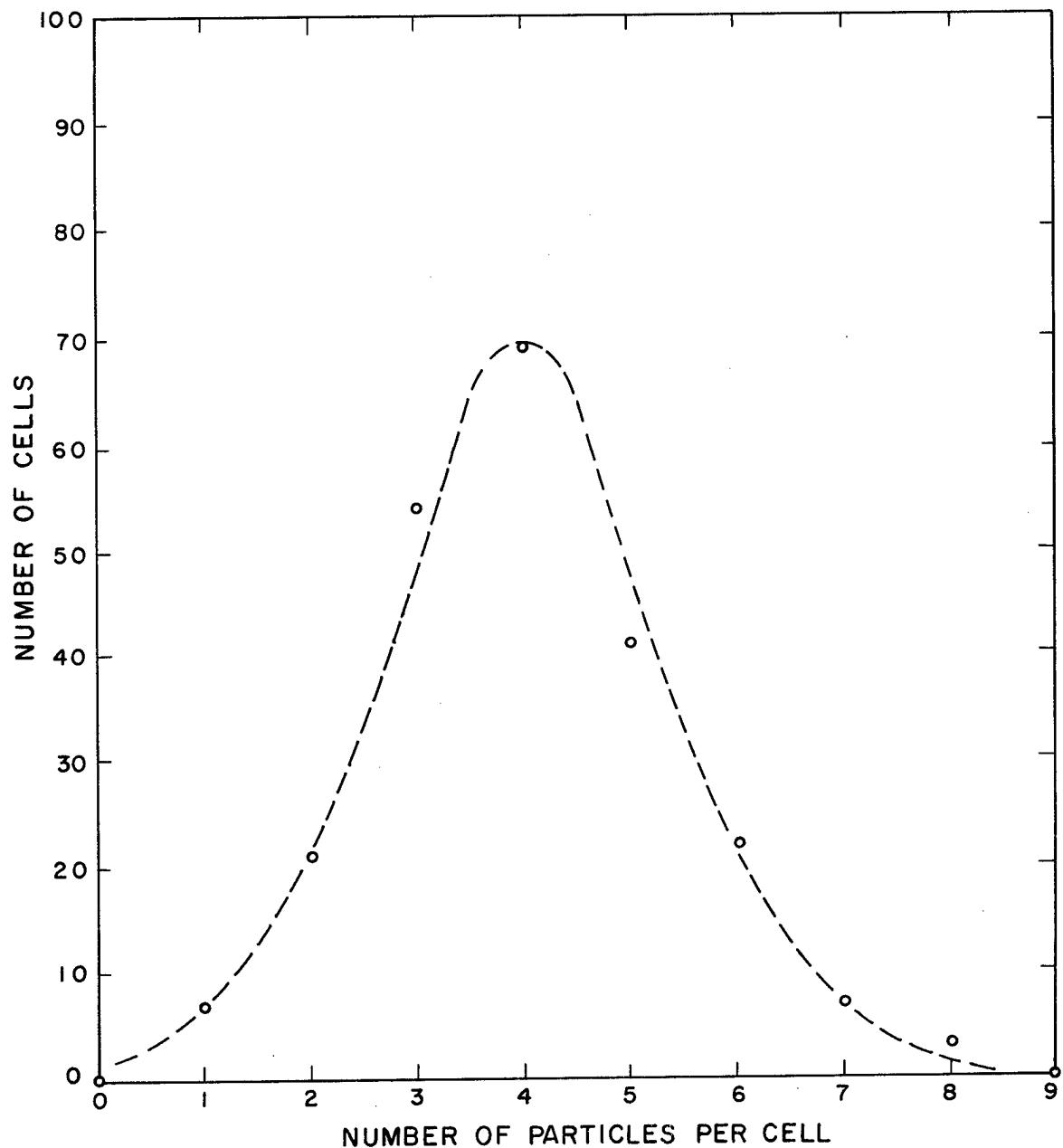
Fig. 25  Distribution of number of particles per cell at t = 67.5 in the perturbed-stagnation problem.  Individual values are as obtained from the calculation; dashed curve probably is close to the final equilibrium distribution.
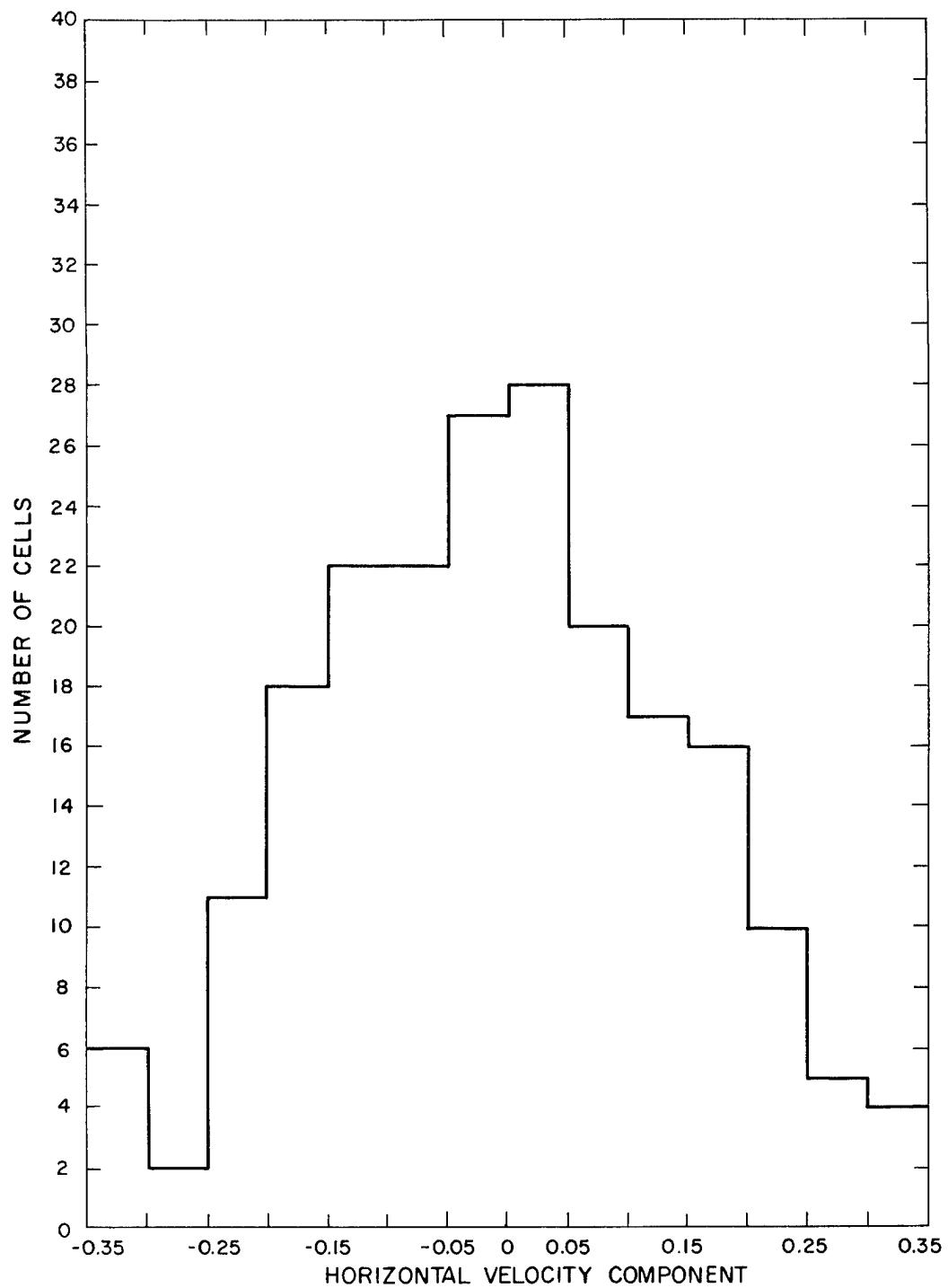
Fig. 26   Distribution of horizontal component of velocity at t = 67.5 in the perturbed-stagnation problem.  A few cells with values outside the ranges shown were not included.
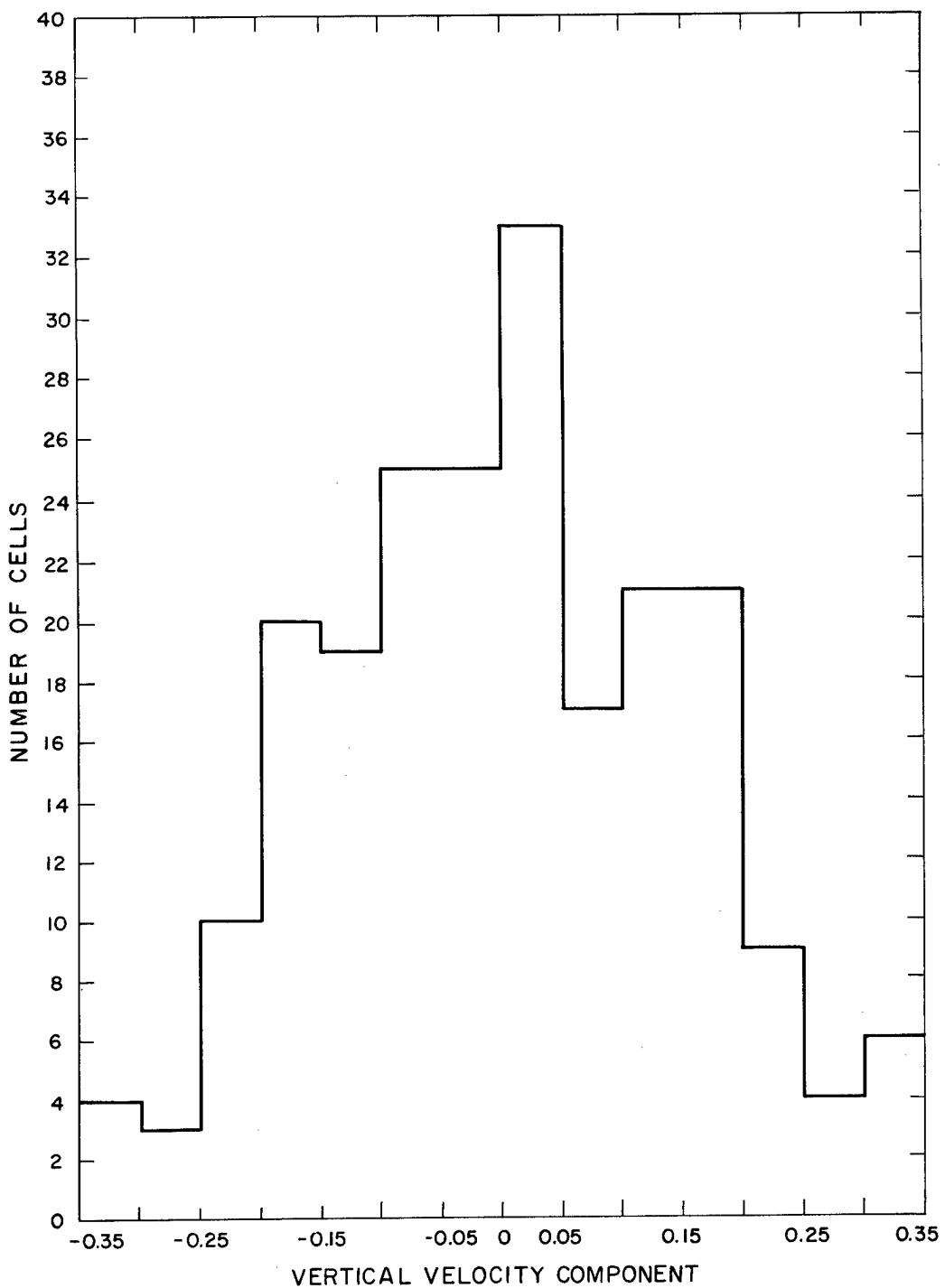
Fig. 27 Distribution of vertical component of velocity at t = 67.5 in the perturbed-stagnation problem. A few cells with values outside the ranges shown were not included.
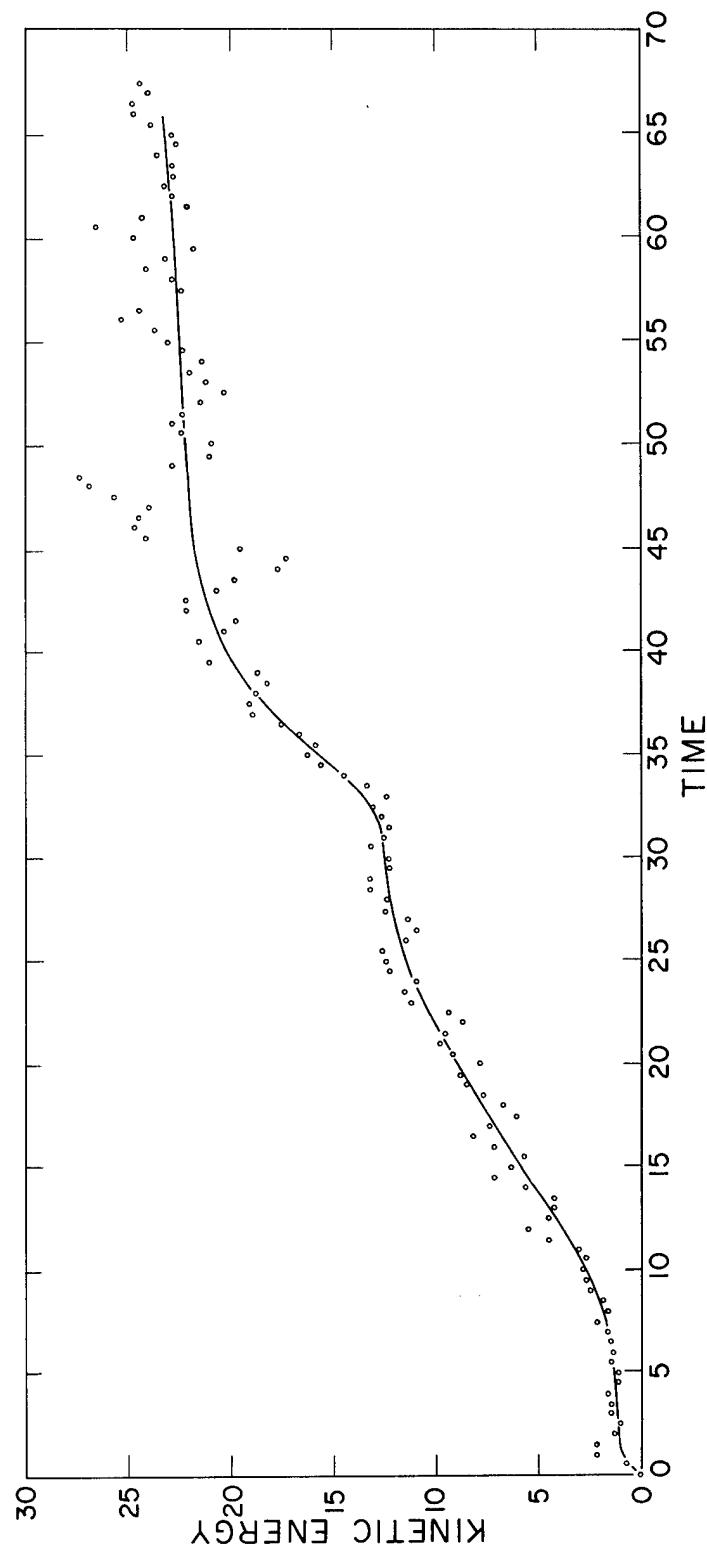
Fig. 28   Total kinetic energy of the gas as a function of time in the perturbed-stagnation problem.
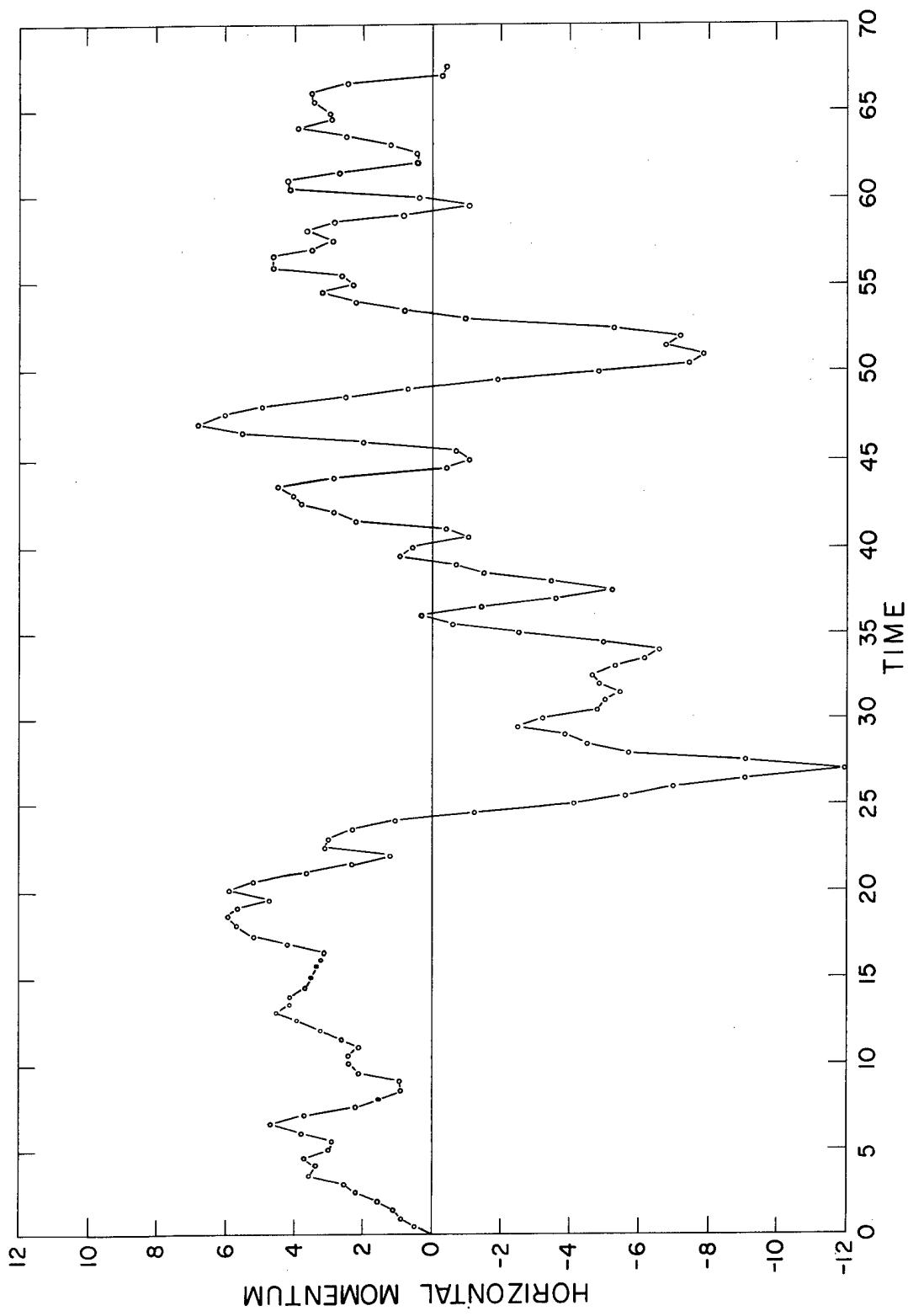
Fig. 29 Total horizontal momentum of the gas as a function of time in the perturbed–stagnation problem.